SARS-CoV-2 infection of human brain microvascular endothelial cells leads to inflammatory activation through NF-κB non-canonical pathway and mitochondrial remodeling

Silvia Torices

  University of Miami Miller School of Medicine

Carolline Motta

  Fundacao Oswaldo Cruz

Barbara da Rosa

  Fundacao Oswaldo Cruz

Anne Marcos

  Fundacao Oswaldo Cruz

Liandra Alvarez-Rosa

  Fundacao Oswaldo Cruz

Michele Siqueira

  Universidade Federal do Rio de Janeiro

Thaidy Moreno-Rodriguez

  University of California San Francisco

Aline Matos

  Laboratório de Vírus Respiratório e do Sarampo, Instituto Oswaldo Cruz, Fundação Oswaldo Cruz,
FIOCRUZ, Rio de Janeiro, Brazil

Braulia Caetano

  Fundacao Oswaldo Cruz

Jessica Martins

  Fundacao Oswaldo Cruz

Luis Gladulich

  Fundacao Oswaldo Cruz

Erick Loiola

  Fluminense Federal University   https://orcid.org/0000-0002-7926-795X

Olivia Bagshaw

  Brock University

Jeffrey Stuart

  Brock University

Marilda Siqueira

Oswaldo Cruz Foundation

Joice Stipursky

Universidade Federal do Rio de Janeiro

Michal Toborek

University of Miami   https://orcid.org/0000-0003-4475-2119

Daniel Adesse (✉ daniel.adesse@gmail.com)

Instituto Oswaldo Cruz   https://orcid.org/0000-0002-7421-9510

Article

Keywords:

Abstract

Neurological effects of COVID-19 and long-COVID-19 as well as neuroinvasion by SARS-CoV-2 still pose several questions and are of both clinical and scientific relevance. We described the cellular and molecular effects of the human brain microvascular endothelial cells (HBMECs) *in vitro* infection by SARS-CoV-2 to understand the underlying mechanisms of viral transmigration through the Blood-Brain Barrier. Despite the low to non- productive viral replication, SARS-CoV-2-infected cultures displayed increased apoptotic cell death and tight junction protein expression and immunolocalization. Transcriptomic profiling of infected cultures revealed endothelial activation via NF-κB non-canonical pathway, including RELB overexpression, and mitochondrial dysfunction. Additionally, SARS-CoV-2 led to altered secretion of key angiogenic factors and to significant changes in mitochondrial dynamics, with increased mitofusin-2 expression and increased mitochondrial networks. Endothelial activation and remodeling can further contribute to neuroinflammatory processes and lead to further BBB permeability in COVID-19.

Introduction

Coronavirus disease 2019 (COVID-19), caused by infection with severe acute respiratory syndrome-related coronavirus 2 (SARS-CoV-2) remains at major health threat globally. The U.S. continues to lead the world with a total of 47.9 million COVID-19 cases and 773,887 deaths at the end of November 2021 (WHO). Even though vaccines, which mostly prevent serious illness and death, have been widely available in the U.S. and many countries, only 59% of the overall population are fully vaccinated. This is below the estimated 85–90% threshold assumed to be needed to stop the spread of SARS-CoV-2 and make the virus endemic. Globally, COVID-19 cases continue rising, and new variants and subvariants (e.g. omicron BA.1, BA.2 [BA.2.12, BA.2.12.1]) were recently identified in different countries, spreading globally (WHO, 2022).

SARS-CoV-2 is a member of the family of β-coronaviruses, similar to two other highly pathogenic coronaviruses: severe acute respiratory syndrome coronavirus (SARS-CoV) and Middle East respiratory syndrome coronavirus (MERS-CoV). Initial SARS-CoV-2 infection cases investigated led to the isolation of the virus in human respiratory epithelial cells (CDC; Zhu et al., 2020) and its genome sequencing deposited (GISAID accession IDs: EPI_ISL_402119, 402120 and 402121). SARS-CoV-2 is an enveloped, positive-sense, and single-stranded RNA virus. Its genome encodes non-structural proteins (such as 3-chymotrypsin-like protease, papain-like protease, helicase, and RNA-dependent RNA polymerase; all key enzymes in the viral life cycle), structural proteins (spike [S] protein, membrane [M] protein, envelope [E] protein and nucleocapsid [N] protein) and accessory proteins.

It is now known that SARS-CoV-2 infects human cells through the ligation of the S1 subunit of the S protein with host cell receptors, especially the angiotensin-2 converting enzyme (ACE2), that serves as an entry receptor to the virus, representing its main route of entry into the host cell (Wang et al., 2020). Pulmonary, cardiac and intestinal epithelia and endothelial cells express high levels of ACE-2 (CDC,

2020). Upon S1-ACE2 interaction, a transmembrane serine protease 2 (TMPRSS2) is required for priming of the S protein and viral entry into the cell (Coronaviridae Study Group of International Committee on Taxonomy of Viruses, 2020; Zhu et al., 2020; Ni et al., 2019). Along with ACE2 and TMPRSS2, several other proteins have been suggested to participate in SARS-CoV-2 entry into human cells, such as ADAM metallopeptidase domain 17 (ADAM17) (Torices et al, 2021; Hoffmann et al., 2020), dipeptidyl peptidase 4 (DPP4) (Zhou et al., 2020; Shulla et al., 2011), angiotensin II receptor type 2 (AGTR2) (Zipeto et al., 2020; Schreiber et al., 2020), basigin (BSG, also called extracellular matrix metalloproteinase inducer [EMMPRIN] or cluster of differentiation 147 [CD147]) (Solerte et al., 2020; Bassendine et al, 2020), aminopeptidase N (ANPEP) (Cui et al., 2020) and cathepsin B/L (de Souza et al. 2020; Wang et al., 2020).

Among the symptoms most commonly observed in COVID-19 patients, alterations of neural functions are frequently detected, from mild cases with loss of taste and smell, dizziness and headaches, to more extreme cases with occurrence of acute cerebrovascular disease, including episodes of vascular encephalic accidents, loss of consciousness, ataxia and epilepsy (Qiao et al., 2020). The Central Nervous System (CNS)-related symptoms are also prominent for so called chronic or long-COVID. The CNS is a well-documented target of β-coronavirus infections, such as SARS-CoV-2, and to date several studies detected SARS-CoV-2 in the brain and the cerebrospinal fluid of COVID-19 patients (Qi et al., 2020; Padmanabhan et al., 2020; Istlfl et al., 2020; Ellul et al., 2020). Distinct routes of SARS-CoV-2 entry into the brain have been proposed, such as the olfactory nerve (Mao et al., 2020; Solomon et al., 2020; Virhammar et al., 2020), the choroid plexus and the blood-brain barrier (BBB) (Baig et al., 2020). However, the contribution of the BBB may be particularly important due to presence of the virus in the bloodstream allowing the passage of viral particles through the wall of brain capillaries to brain parenchyma. While the mechanisms of SARS-CoV-2 neuroinvasion are not fully understood, it has been suggested that infection of BBB capillaries-composing cells is critical to trigger CNS impairment (Li et al., 2020a; Li et al., 2020b). Several essential characteristics that ensure BBB function are supplied by endothelial cells that express specific types of tight junction proteins (Briguglio et al., 2020; Alam et al., 2020; Achar et al., 2020).

Several reports have correlated the infection outcome with vascular dysfunction, establishing vascular inflammation and cytokine storms promoted by immune responses as critical factors contributing to worsening of the clinical condition and even death. Endothelial dysfunction may have important consequences, which include ischemia, altered angiogenesis and coagulation, inflammation, and tissue edema. Therefore, COVID-19-related endothelitis could explain the systemic microcirculatory dysfunction observed in patients, including chronic form of this disease. It was recently demonstrated that the treatment of human brain microvascular endothelial cells with recombinant S1 protein resulted in endothelial permeability and altered the levels of pro-inflammatory cytokines (Buzhdygan et al., 2020). However, little is known about the involvement of brain microvasculature in brain infection by SARS-CoV-2, which may result in endothelial activation and hyper-inflammatory responses. Even less is known if damages to the BBB could be propagated to neural tissue, and therefore be the triggering mechanism of neural abnormalities that promote neurological symptoms observed in COVID-19 patients.

In the present work we describe cellular and molecular effects of HBMEC infection by SARS-CoV-2 in order to gain insight into possible routes by which the virus affects the BBB and invades the brain parenchyma. Transcriptomic analyses revealed activation of noncanonical NF-κB signaling pathway and changes in mitochondrial quality control, which combined could induce endothelial activation and promote increased neuroinflammation in Neuro-COVID-19.

Methods

1. Cell culture

Human brain endothelial cells (HBMECs) were a gift from Prof. Dennis Grab (Department of Pathology, Johns Hopkins School of Medicine). Cells were immortalized using a SV40-LT plasmid (Stins et al., 2001) and were maintained in 199 medium with 10% fetal bovine serum (FBS) and 1% antibiotics (penicillin/streptomycin, ThermoFisher) up to passage 38. Vero E6 cells (African green monkey kidney epithelial cells) were used as gold standard for viral isolation and propagation and were used in a few experiments as a positive control for efficient SARS-CoV-2 infection. Vero E6 cells culture medium consisted of Dulbecco's Modified Eagle Medium (DMEM) formulated with D-glucose (4.5 g/l) and L-Glutamine (3.9 mM) supplemented with 100× penicillin-streptomycin solution (to final 100 U/ml and 100 µg/ml, respectively) and with inactivated FBS (USDA-qualified region FBS) at 10%. Both cell and viral cultures were incubated at 37°C and 5% CO_2.

2. SARS-CoV-2 isolate

All the procedures associated to the viral culture and further infection assays were performed in biosafety level 3 laboratory, in accordance with the WHO guidelines (WHO, 2021). The SARS-CoV-2 isolate used in this study was previously obtained from a respiratory sample collected from a COVID-19 patient diagnosed in March 2020, in Brazil, as part of the Brazilian Ministry of Health surveillance system. Viral isolation and genetic characterization were previously described (Matos et al, 2022). All procedures involving patient samples were approved by the Committee of Ethics in Human Research of the Oswaldo Cruz Institute (registration number CAAE 68118417.6.0000.5248).

3. SARS-CoV-2 infection

Cells were cultured to obtain confluent monolayers. After that, cells were washed once with PBS and SARS-CoV-2 inoculums corresponding to indicated multiplicities of infection (MOI) were incubated for one hour. After infection, inoculums were removed from cells and replaced by their appropriate supplemented medium with TPCK treated trypsin at 1 µg/mL.

4. Viral quantification

We evaluated SARS-CoV-2 replication of infected cells over time by measuring the number of viral RNA copies in their culture media over time. Viral RNA was extracted from 140 µL of cell-free culture media using QIAamp Viral RNA mini kit (Qiagen, Germany), according to manufacturer's instructions. Reverse

transcription and SARS-CoV-2 gene amplification were performed in one-step reactions with a quantitative real time PCR kit developed by Biomanguinhos Institute (Fiocruz, Brazil), in an ABI 7500 thermocycler (Applied Biosystems, USA). As a quantification standard, we used a SARS-CoV-2 plasmid control containing the reference sequence of viral envelope (E) gene, with a known number of copies (IDT, USA). Therefore, a concentration curve was prepared by performing serial dilutions of the plasmid.

5. RNA libraries and sequencing

For RNAseq analysis, three independent replicates were prepared for each treatment groups: Mock, MOI 0.01- and MOI 0.1-infected cultures, at 6 and 24 hpi. Total RNA was isolated using the miRNeasy micro kit (Qiagen) according to the manufacturer's instructions. The RNA was quantified by O.D. measurement before being assessed for quality by chip-based capillary electrophoresis using Agilent 2100 Bioanalyzer RNA 6000 Pico assays (Agilent Technologies; Part # 5067 – 1513).

Libraries were prepared from 150 nanograms (ng) of DNA-free total RNA using the Universal Plus mRNA-Seq Library Prep Kit (NuGEN Technologies, Inc.; Part # 0508 – 96). The quality and size distribution of the amplified libraries were determined by chip-based capillary electrophoresis on Agilent 2100 Bioanalyzer High Sensitivity DNA assays (Agilent Technologies; Part # 5067 – 4626). Libraries were quantified using the Takara Library Quantification Kit (Part # 638324). The libraries were pooled at equimolar concentrations and diluted prior to loading onto a P3 flow-cell (Illumina; Part # 20027800) with the P3 300 Cycle reagent kit (Illumina; Part # 20038732) on the NextSeq2000 instrument.

6. RNA-seq data analysis

Reads R1 and R2 were trimmed 12 nucleotides (nt) to remove low quality sequences. Bases with a quality score of less than Q20 were trimmed off the right end of each R1 and R2. Illumina adapter sequences were trimmed from the 3'-end of both R1 and R2 reads. Read pairs in which mate in the pair was less than 30nt after trimming were discarded. These quality-filtered reads were then used for alignment.

Sequence alignment was performed using HISAT2 (https://doi.org/10.1038%2Fnmeth.3317) version 2.0.5 with the following settings:

hisat2 --end-to-end -N 1 -L 20 -i S,1,0.5 -D 25 -R 5 --pen-noncansplice 12 --mp 6,3 --sp 3,0 --time --reorder --known-splicesite-infile [SPLICESITES] --novel-splicesite-outfile splicesites.novel.txt --novel-splicesite-infile splicesites.novel.txt -q --x [hsa38 HISAT2 INDEX] -1 [FASTQ1] -2 [FASTQ2] -S [SAMOUT]. The read summarization program featureCounts (https://academic.oup.com/bioinformatics/article/30/7/923/232889) version 1.5.1 was used for exon- and gene-level counting. An Ensembl human version 83 GTF file (downloaded from Ensembl Biomart on January 22, 2016) was used for determination of exon boundaries and the exon-gene relationship during counting. The summarization level used for exon and gene counting was the feature and the meta-feature, respectively. featureCounts is available in the Subread package at http://subread.sourceforge.net/ (https://academic.oup.com/nar/article/47/8/e47/5345150?login=true).

To determine differential gene expression and due the low coefficient of biological variation, paired comparisons were performed between the untreated control and MOIs 0.01 and 0.1 treated HBMEC cells at 6 and 24 hrs timepoints, using an additive linear model with untreated group as the blocking factor. Differential gene expression analysis was performed using EdgeR R package (https://academic.oup.com/bioinformatics/article/26/1/139/182458).

The top differentially expressed genes have consistent UC vs MOIpt1 changes for the three replicates at 5% FDR, and absolute log2 fold change of 0.6 were considered cut-offs to generate the DEG list. Computed z-scores of significant genes are represented in the heatmap. Heatmap was plotted using complexheatmap R package. (https://academic.oup.com/bioinformatics/article/32/18/2847/1743594).

7. Downstream RNA-seq analysis

We used a list of genes differentially expressed between MOI 0.1 SARS-CoV-2-infected and uninfected HBMEC cells. The pathway enrichment and interaction networks analysis were performed using clusterProfiler and gprofiler2 R packages (https://www.sciencedirect.com/science/article/pii/S2666675821000667, https://f1000research.com/articles/9-709/v2). Overlapping gene sets from reactome pathway terms, were visualized as a chord plot using the GOplot R (https://academic.oup.com/bioinformatics/article/31/17/2912/184136).

8. RT-qPCR

Cells were grown in 60 mm^2 dishes and total RNA was extracted with Trizol reagent (Thermo Fisher), according to the manufacturer's instructions. One microgram of total RNA was reversely transcribed into cDNA using SuperScript III system (Thermo Fisher) and 0.5 μl of cDNA was used per RT-qPCR reaction with Power SYBR Green (Thermo Fisher) master mix. Reactions were read in 7500 StepOne Plus from the Oswaldo Cruz Institute. Primer sequences for Drp1, Fis1, ZO-1, claudin-5, HIF-1α, Mfn2, MFF and TOMM20 are provided in **Table S1**. For E gene and Spike1 RT-qPCR, we used the protocols described in Corman et al., 2020 and Won et al., 2020, respectively. For the remaining genes, 100 ng of total RNA was used for Taqman reactions using primer probes from Thermo Fisher: Hs00242739_m1 (LTB), Hs00174128_m1 (TNF), Hs00232399_m1 (RELB), Hs00357891_s1 (JUNB), Hs00759776_s1 (FOSL1), Hs00765730_m1 (NFKB1), Hs00174103_m1 (CXCL8), Hs00601975_m1 (CXCL2), Hs00236937_m1 (CXCL1), Hs00173615_m1 (PTX3), Hs00174961_m1 (EDN1), Hs00299953_m1 (SERPINE2) and Hs01028889_g1 (NFKB2). GAPDH (Hs02786624_g1) was used for sample normalization. Gene expression variations were assessed by the $2^{\Delta\Delta Ct}$ method, with Ct as the cycle number at threshold. Desired PCR result specificity was determined based on melting curve evaluation.

9. Western blotting

HBMECs were cultivated in 60 mm^2 dishes and at desired times were washed with PBS and lysed in the presence of 1x Laemmli Buffer (0.0625M Tris, 0.07M SDS, 10% glycerol, 5% β-mercapto-ethanol and bromophenol blue). Protein concentration was measured with BCA Protein Assay Kit according to the

manufacturer's instructions (Thermo Fisher Scientific, Carlsbad, CA, USA). Then, 30 µg of protein were loaded onto 4–20% gradient acrylamide gels (Bio-Rad Laboratories, Hercules, CA, USA). Membranes were blocked with bovine serum album (BSA) 5% in TBS-0.05% Tween20 and incubated overnight at 4°C with the primary antibodies at 1:1,000 dilution in TBST (**Table S2**). Next day, blots were washed with TBS-0.05% Tween20, incubated for 1 hour at room temperature with secondary antibodies (Lincoln, NE, USA) and analyzed using the Licor CLX imaging system and the Image Studio 4.0 software (LI-COR).

10. Immunofluorescence

Cells were grown on 13-mm round glass coverslips and fixed at desired times with 4% paraformaldehyde in PBS for 10 min at 20ºC, permeabilized with 0.5% Triton x-100 (Sigma Aldrich), blocked with 3% bovine serum albumin (BSA, Sigma Aldrich) and incubated overnight with primary antibodies at 4 ºC. Cells were washed with PBS and incubated with fluorescently labeled secondary antibodies for 1 h at 37 ºC. For nuclear visualization, cells were incubated with DAPI (4',6-diamidino-2-phenylindole) and mounted in a solution of glycerol and DABCO (1,4-diazabicyclo[2.2.2]octane) in PBS. The list of primary and secondary antibodies used in this study are detailed in **Table S2**.

11. Quantitative analysis of mitochondrial network morphology

Mitochondrial network morphology was analyzed using the Mitochondrial Network Analysis Tool (MiNA) for the Fiji distribution of ImageJ (Valente et al. 2017). Images were cropped into individual cells. To enhance contrast and sharped mitochondrial images, several pre-processing tools were applied to each image prior to MiNA analysis. First, an unsharp mask (sigma = 3) was used to sharpen images by subtracting a blurred version of the image (i.e. unsharp mask) from the image. The unsharp mask is created by Gaussian blurring the original image and multiplying the blurred image by the mask weight (0.8). Second, a median filter (radius = 1) was applied to each image. The median filter functions by replacing each pixel with the neighborhood median, where the neighborhood size is determined by the radius. Following pre-processing, images underwent thresholding using the Otsu thresholding to produce a binary image (Otsu, 1979). The mitochondrial footprint is calculated as the total number of mitochondria-signal positive pixels from the binarized image. A morphological skeleton is then produced from the binarized image using the Skeletonize 2D/3D plug-in (Arganda-Carreras et al. 2010; Lee et al. 1994). This method employs iterative thinning to create a skeleton of mitochondrial structures, one pixel wide. Length measurements of the mitochondrial structures are then measured using the Analyze Skeleton plug-in, resulting in two additional parameters: mean branch length and mean summed branch length. Mitochondrial form branching networks, in which branches intersect at a node. Mean branch length is calculated as the mean length of mitochondrial structure between two nodes. Mean summed branch length is calculated by determining the sum of branch lengths within an independent network structure and dividing by the total number of independent networks within a cell.

12. Angiogenesis-related proteins secretome

For generation of HBMEC Conditioned Medium (CM), cells were plated on 6-well plates and after infection were maintained in a total volume of 1 ml per well. Conditioned culture media were collected at 24 hours post infection (hpi) and centrifuged for 5 min at 10,000 rpm at 4 ºC and stored at -80 ºC until use. Secretion of angiogenesis-related protein levels was detected using a Proteome Profiler™ Human Angiogenesis Antibody Array kit (R&D Systems) according to manufacturer's instructions. Membranes were incubated with pools of two independent experiments (e.g.: Mock #1 + Mock #2, MOI 0.01 #1 + MOI 0.01 #2, etc.) for each experimental condition, in a total of 3 membranes for 6 biological replicas. Spots were detected with chemoluminescence and X-ray films were exposed for 1, 5, 10 and 15 minutes to detect differentially expressed proteins. Densitometric analysis was performed with UN-SCAN-IT gel analysis software and relative intensity values for each spot of the 1-minute exposed film was analyzed with GraphPad Prism software version 9.0.1.

13. Transmission electron microscopy

Cells were grown on 35 mm petri dishes and infected or treated as described above. At desired time, cultures were washed in PBS, fixed with 2.5% glutaraldehyde diluted in 0.1 M cacodylate buffer with 3.5% sucrose and $CaCl_2$ for 1 h at 20 ºC, followed by washes in cacodylate buffer and post-fixation with 1% osmium tetroxide with potassium ferricyanide for one hour at 4 ºC in the dark. Cells were dehydrated in crescent acetone gradient and embedded in Epon resin at 60ºC for 72 h. Ultrathin sections were obtained with Leica ultramicrotome and collected in 300-mesh copper grids, stained with uranyl acetate and lead citrate and visualized at Hitachi Transmission Electron Microscope at Centro Nacional de Bioimagem (CENABIO-UFRJ).

14. Statistical analyses

For RT-qPCR and western blotting, a minimum of 5 independent cell culture preparations were used and analyzed with Two-Way ANOVA with Bonferroni post-test in GraphPad Prism Software v9.3.1. Morphometrical analysis of ZO-1 immunostaining were performed with ImageJ software for fluorescence intensity and Tight Junction Organization Rate (TiJOR) using the TiJOR macro for ImageJ, which in an index of localization of tight junction proteins in membrane-membrane contact region of adjacent cells as described by (Terryn et al. 2013).

Results

1. Characterization of HBMEC infection by SARS-CoV-2

In order to characterize the profile of host cell infectivity by SARS-CoV-2, HBMEC and Vero E6 cells were infected in the presence or not of serine endoprotease TPCK trypsin (1 µg/ml), which was shown to increase infectivity in Calu-3 cells, a permissive cell line for the efficient replication of SARS-CoV-2 (Jiang et al., 2021). Cultures were infected at different multiplicities of infection (MOIs) of 0.01, 0.1, 1 and 2 and supernatants were collected at 6-, 24-, 48- and 72-hours post-infection (hpi) and analyzed by RT-qPCR for quantification of viral E gene (Fig. 1A). We found that HBMECs showed no increase in viral replication or

release in the supernatant over time, whereas Vero E6 cells had time-dependent release of SARS-CoV-2 in the supernatant, as expected (Fig. 1A). TPCK trypsin treatment did not affect the cell infectivity rates; however, for consistency, all subsequent assays were performed in the presence of TPCK. In the same context, HBMECs infected with different MOIs did not show any increase in the expression of SARS-CoV-2 Spike1 and E genes at 6 and 24 hpi (Fig. 1B). We showed recently that HBMEC cells express, to some extent, several of SARS-CoV-2 receptors at both RNA and protein levels (Torices et al., 2021). Therefore, we evaluated the possible effect of infection on the expression of ACE2 and TMPRSS2 in HBMEC cells and found that infection with the MOI 0.1 induced a 40% decrease in ACE2 mRNA expression (p < 0.05), which did not result in ACE2 protein level alterations (Fig. 1C). However, TMPRSS2 showed a 1.77-fold increase in protein levels in MOI 0.1-infected cultures at 24 hpi (p = 0.078). Despite the apparent non-productive infection of HBMEC, SARS-CoV-2 was able to induce apoptosis of HBMECs, as detected by cleaved caspase-3 immunostaining (Fig. 1D) at 24 hpi. MOIs 0.01 and 0.1 resulted in 2.27 and 4.1% of caspase-3-positive cells, respectively, whereas non-infected dishes showed a physiological rate of 0.7% of stained cells. Apoptotic stimulus was also observed in Vero E6 cells 24 hpi with MOI 0.1 (Fig. 1D). Positive control with 0.5 and 2.0 μg Staurosporine for 2 hours led to 1.9 and 9% of caspase-3 positive HBMECs, respectively (not shown).

2. SARS-CoV-2 affects tight junction genes expression in BBB-forming cells

The barrier property of BMECs is mostly conferred by the expression and function of tight junction proteins, such as ZO-1 and claudin-5 (Takata et al., 2021). HBMEC and Vero E6 cells were infected as described above and analyzed at 6 and 24 hpi. ZO-1 immunoreactivity was drastically altered in infected Vero cultures (Fig. 2A) and showed discontinuous staining in cell-cell contacts, as compared to uninfected controls. SARS-CoV-2 viral particles were clearly detected in Vero cells as revealed by Spike1 immunoreactivity. Conversely, infected HBMEC cultures did not present as significant differences in distribution of ZO-1 along cells membranes at 24 hpi (Fig. 2A). To better evaluate ZO-1 organization in TJ we performed densitometric (ZO-1 fluorescence intensity) and tight junction organization rate (TiJOR) (Terryn et al. 2013) analyses. We observed that ZO-1 presented a significant 1.29-fold increase in TiJOR index with MOI 0.1 at 6 hpi, concomitantly with a 1.3-fold increase in fluorescence signal, and such effects were lost 24 hpi. In parallel, MOI 0.01 affected ZO-1 fluorescence signal at 24 hpi by 1.19-fold (Fig. 2B). ZO-1 and claudin-5 mRNA expression remained unaltered throughout the infection (Fig. 2C), but their protein levels were significantly increased by 2.0- and 1.17-fold by the MOI 0.1 at 24 hpi, respectively (Fig. 2D).

3. SARS-CoV-2 infection promotes endothelial activation and hyper-inflammatory response in vitro

We determined the transcriptional profile of HBMECs after SARS-CoV-2 infection by RNA-Seq after 6 and 24 hpi. At 6 hpi, biological replicas had high variability across experiments, as determined by the square root of the common dispersion and visualized by principal component analysis (not shown). Infection with both MOIs 0.01 and 0.1 led to minimal effect on HBMEC's transcriptome, with few significantly

differentially expressed genes (DEGs) and no pathways enrichment found (Supplementary material). However, at 24 hpi we observed significant impact on host cell transcriptome: exposure to SARS-CoV-2 MOI 0.1 led to up-regulation of 23 and down-regulation of 4 genes. Volcano plot and heatmap on Fig. 3 (**A-B**, respectively) depict the transcriptomic profile of HBMECs infected with the MOI 0.1 at 24 hpi. Data obtained from RNA-Seq was consistent with an endothelial activation, with high expression levels of cytokines (IL-6, IL-8, TNF) and chemokines (CXCL1, -2, -8 and CCL20) encoding genes (Fig. 3). Accordingly, functional enrichment analysis revealed that main genes found related to "Cytokine signaling in immune system", "TNF signaling" and "TNFR1-induced NFkappaB signaling pathway", among other Reactome terms (Fig. 3C). In fact, TNF was the most up-regulated gene, with 104-fold increase, followed by TNF-c (Lymphotoxin beta, LTB), with 32.8-fold change (Fig. 3, Table 1). Interestingly, LTB is a known inducer of noncanonical NFκB inflammatory pathway (Mockenhaupt et al., 2021) and was found to be up-regulated both at 6 and 24 hpi in SARS-CoV-2 infected HBMEC by RT-qPCR (Fig. 3E). Although our RNA-Seq data revealed an increase in NFκB2 (p100/p52) and NFκBIA (IκBα), we performed RT-qPCRs with additional biological samples for NF-κB1 (p105/p50) and NF-κB2 and observed that, due to biological variability, such genes remained unaltered in infected cultures (Fig. 3D). However, RELB, the main activator of noncanonical NF-κB signaling pathway (Mockenhaupt et al., 2021), was shown to be up-regulated by confirmatory RT-qPCR at 24 hpi (Fig. 4). We also further confirmed by RT-qPCR the up-regulation of inflammation-related genes, including LTB, TNF, IL-6, CXCL1, CXCL2 and CXCL8 (Fig. 3E). Pentraxin3 (PTX3) is a glycoprotein involved in the innate immune response and has a relevant role in FGF2-dependent angiogenesis (reviewed in Presta et al., 2018). We found that PTX3 to be 19.6-fold increased in SARS-CoV-2 infected HBMECs (Figs. 3A and 4). Apart from the inflammatory transcriptomic response, KEGG pathways related to ribosomal structure/function and mitochondrial biology were found to be altered by SARS-CoV-2-infected HBMECs at 24 hpi (Fig. 3D).

Table 1

Differentially expressed genes in MOI 0.1-infected HBMEC cultures at 24 hpi.

Gene name	Symbol	Fold-change (log)	P value	FDR
Uncategorized gene	RP11-298I3.3	-2.19	0.00001795234598	0.04214061886
ankyrin repeat domain 36C	ANKRD36C	-1.42	0.000000005528613831	0.00002495701339
upstream transcription factor family member 3	USF3	-0.76	0.00002036226065	0.04595918861
SMG1 nonsense mediated mRNA decay associated PI3K related kinase	SMG1	-0.75	0.000002651386726	0.007779698933
nuclear factor kappa B subunit 2	NFKB2	0.64	0.00002117775188	0.04602945153
E74 like ETS transcription factor 3	ELF3	0.82	0.00001027948854	0.02601045479
ephrin A1	EFNA1	0.82	0.0000001766175517	0.0006096837885
Epstein-Barr virus induced 3	EBI3	0.87	0.000005771957935	0.01612959902
intercellular adhesion molecule 1	ICAM1	0.97	0	0.0000005593411357
complement C3	C3	1.01	0.000000004506547278	0.00002203851837
NFKB inhibitor alpha	NFKBIA	1.05	0	0.00000008288304584
C-C motif chemokine ligand 2	CCL2	1.14	0.000000002315586268	0.00001235344223
baculoviral IAP repeat containing 3	BIRC3	1.27	0.00000002052506134	0.00007528079373
zinc finger CCCH-type containing 12A	ZC3H12A	1.29	0	0.0000003145723235

Gene name	Symbol	Fold-change (log)	P value	FDR
RELB proto-oncogene, NF-kB subunit	RELB	1.30	0	0.00000008288304584
Uncharacterized protein	AC010646.3	1.31	0.0000103901062	0.02601045479
interleukin 6	IL6	1.36	0	0.00000002581261588
TNF alpha induced protein 3	TNFAIP3	1.38	0.00000001761165902	0.00006890150651
TNF alpha induced protein 2	TNFAIP2	1.42	0.000001921435199	0.005934605433
C-X-C motif chemokine ligand 2	CXCL2	1.79	0	0
TNF superfamily member 18	TNFSF18	1.95	0.0000106374977	0.02601045479
C-X-C motif chemokine ligand 1	CXCL1	2.24	0	0
C-X-C motif chemokine ligand 3	CXCL3	2.32	0.0000000001312489102	0.0000007702211048
C-C motif chemokine ligand 20	CCL20	3.50	0.00000007991169552	0.00003349669957
pentraxin 3	PTX3	4.30	0	0
lymphotoxin beta	LTB	5.04	0	0

4. Angiogenic profiling of SARS-CoV-2-infected HBMEC cells

Dysfunctional angiogenesis is a common phenomenon observed in neuroinflammatory states and can be a result of BBB damage (Estato et al., 2018). We analyzed the profile of angiogenesis-related secreted proteins by HBMECs during infection with SARS-CoV-2 and observed that out of 55 spotted targets, 15 had most significantly detectable signals (Fig. 4A-B, Table 2). Highest signals were observed for uPA, serpin-E1 (PAI-1), IL-8, thrombospondin-1, VEGF, TIMP-1, endothelin-1 (ET-1), PTX3, angiogenin and amphiregulin, with at least 5,000 pixels each. SARS-CoV-2-infected cultures (MOI 0.1) had most pronounced increase in secretion of PTX-3 and TIMP-1 as compared to Mock cultures, with 113 and

112% levels, respectively. Accordingly, PTX-3 was also one of the most up-regulated genes as determined by RNA-Seq (Fig. 3). We further assessed the expression levels of PTX3 by RT-qPCR and found it to be increased in HBMEC cultures after 6 and 24 hpi with the MOI 0.1, whereas VEGF, Serpin-E2 and ET-1 showed no significant changes at the transcriptional level (Fig. 4C). Insulin-like growth factor (IGF) binding protein-3 (IGFBP-3), a member of the IGFBP family was shown to be 166 and 125% more abundant in the HBMEC conditioned media in MOI 0.01 and 0.1-infected dishes, respectively. We performed scratch-wound healing migration assays in infected HBMECs, however no effect in cellular migration was noticed in infected cultures as compared to Mock-infected (not shown). Interestingly, hypoxia-inducible factor-1 alpha (HIF-1α) was also increased by SARS-CoV-2 at both MOIs at 24 hpi (Fig. 4C).

Table 2
Differentially secreted angiogenic proteins in SARS-CoV-2-infected HBMECs.

Analyte name (alternate nomenclature)	Gene ID	Foreground pixel intensity (*fold change relative to Mock*)		
		Mock	MOI 0.01	MOI 0.1
Activin-A	3624	55.5	32.5 (*0.6*)	88.5 (*1.63*)
ADAMTS-1	9510	25.5	12.5 (*0.52*)	45.5 (*1.88*)
Angiogenin (ANG)	283	6427	7818 (*1.21*)	6553 (*1.01*)
Angiopoietin-1 (Ang-1)	284	147	86 (*0.59*)	155 (*1.07*)
Angiopoietin-2 (Ang-2)	285	39.5	12 (*0.32*)	79.5 (*2.08*)
Angiostatin/ Plasminigen	5340	144.5	10 (*0.07*)	74 (*0.52*)
Amphiregulin (AR)	374	5797	6744 (*1.16*)	5064.5 (*0.87*)
Artemin	9048	144.5	143 (*0.99*)	64 (*0.46*)
Coagulation Factor III (TF)	2152	818	887 (*1.08*)	622 (*0.76*)
CXCL16	58191	3387.5	3976.5 (*1.17*)	2521.5 (*0.74*)
DPPIV (CD26)	1803	72.5	1.5 (*0.03*)	203 (*2.83*)
EGF	1950	16.5	18 (*1.15*)	40.5 (*2.60*)
EG-VEGF (PK1)	84432	188.5	164 (*0.88*)	257 (*1.38*)
Endoglin (CD105)	2022	17.5	17.5 (*1.05*)	74.5 (*4.40*)
Endostatin/ Collagen XVIII	80781	3827	4747.5 (*1.24*)	3931.5 (*1.02*)
Endothelin-1 (ET-1)	1906	9087.5	9213 (*1.01*)	9007.5 (*0.99*)
FGF acidic (FGF-1)	2246	475	69.5 (*0.15*)	472.5 (*1*)
FGF basic (FGF2)	2247	16.5	5 (*0.36*)	4.5 (*0.42*)
FGF-4	2249	0.5	-1	36.5 (*78.0*)
FGF-7 (KGF)	2252	77.5	15.5 (*0.21*)	180 (*2.34*)
GDNF	2668	101	82 (*0.82*)	105 (*1.06*)
GM-CSF	1437	419.5	275 (*0.65*)	241.5 (*0.58*)
HB-EGF	1839	71	32.5 (*0.47*)	134 (*1.92*)
HGF	3082	10.5	11 (*1.14*)	25.5 (*2.66*)

Analytes in bold had at least 3,000 pixels and were considered as valid signal, as shown in Fig. 4.

Analyte name (alternate nomenclature)	Gene ID	Foreground pixel intensity (*fold change relative to Mock*)		
		Mock	MOI 0.01	MOI 0.1
IGFBP-1	3484	4841.5	4901 (*1.01*)	4684.5 (*0.96*)
IGFBP-2	3485	118	22.5 (*0.19*)	154.5 (*1.33*)
IGFBP-3	3486	3203	5335.5 (*1.66*)	3991 (*1.24*)
IL-1β (IL-1F2)	3553	512	470.5 (*0.92*)	695.5 (*1.36*).
IL-8 (CXCL8)	3576	10875.5	10484.5 (*0.96*)	10744 (*0.98*)
LAP (TGF B1)	7040	292.5	219.5 (*0.75*)	102 (*0.35*)
Leptin	3952	1	44 (*45.0*)	43.5 (*46.0*)
MCP-1 (CCL2)	6347	4549	7624 (*1.67*)	4759 (*1.04*)
MIP-1A (CCL3)	6348	123	103 (*0.84*)	149 (*1.23*)
MMP-8	4317	418	510.5 (*1.22*)	841.5 (*2.01*)
MMP-9	4318	298.5	106.5 (*0.36*)	206 (*0.69*)
NRG1-B1 (HRG1-β1)	3084	256	107.5 (*0.42*)	320 (*1.25*)
Pentraxin-3 (TSG-14)	5806	7509.5	7263.5 (*0.96*)	8523 (*1.13*)
PD-ECGF	1890	441	310 (*0.70*)	600 (*1.36*)
PDGF-AA	5154	1411.5	2129.5 (*1.50*)	1736.5 (*1.23*)
PDGF-AB/ PDGF-BB	5155	923.5	878 (*0.95*)	1161 (*1.25*)
Persephin	5623	565.5	375.5 (*0.66*)	490.5 (*0.87*)
Platelet Factor 4 (CXCL4)	5196	261.5	150.5 (*0.58*)	283.5 (*1.09*)
PIGF	5228	50.5	14 (*0.29*)	90 (*1.83*)
Prolactin	5617	7	49 (*7.14*)	57 (*8.5*)
Serpin B5 (Maspin)	5268	604	578 (*0.95*)	694 (*1.15*)
Serpin-E1 (PAI-1)	5054	10979.5	10955.5 (*0.99*)	11590.5 (*1.05*)
Serpin-F1 (PEDF)	5176	422.5	327.5 (*0.77*)	476 (*1.13*)
TIMP-1	7076	9548	9156 (*0.95*)	10696 (*1.12*)
TIMP-4	7079	446.5	292.5 (*0.65*)	656.5 (*1.47*)

Analytes in bold had at least 3,000 pixels and were considered as valid signal, as shown in Fig. 4.

Analyte name (alternate nomenclature)	Gene ID	Foreground pixel intensity (*fold change relative to Mock*)		
		Mock	MOI 0.01	MOI 0.1
Thrombospondin-1 (TSP-1)	7057	9842	9012 (*0.91*)	9727.5 (*0.98*)
Thrombospondin-2 (TSP-2)	7058	688	929 (*1.35*)	837 (*1.22*)
uPA	5328	12865	13396.5 (*1.04*)	14065 (*1.09*)
Vasohibin	22846	253	172 (*0.68*)	268 (*1.06*)
VEGF	7422	9700.5	9954 (*10.2*)	10559.5 (*1.08*)
VEGF-C	7424	0.5	0	37 (*79.0*)
Analytes in bold had at least 3,000 pixels and were considered as valid signal, as shown in Fig. 4.				

5. Mitochondrial plasticity is affected by SARS-CoV-2 infection

Because mitochondria play a role in cellular homeostasis and pathology, we sought to investigate the effects of SARS-CoV-2 infection on mitochondrial plasticity in HBMECs. Cells were immunostained for mitochondrial import receptor subunit TOMM20 (Fig. 5A). Our first observation was that infection at MOI 0.01 and 0.1 induced a denser mitochondrial network profile, when compared to Mock condition (Fig. 5A-C). MiNA analysis of mitochondrial network organization (Valente et al., 2017), revealed that mitochondrial footprint (Fig. 5C), which measures the mitochondria signal in a 2-dimensional image of a cell, was found to be significantly increased in HBMECs infected with the MOI 0.1 at 6 hpi and with both MOIs at 24 hpi. We next measured mean mitochondrial branch length mean, which is the average length of mitochondrial structures that are either independent or connected to networks (Fig. 5C). We observed a slight, yet significant, increase in cells infected with MOI 0.01 at 6 hpi and with MOI 0.1 at 24 hpi, with a 7 and 3% increase, respectively. Furthermore, MiNA analysis revealed that SARS-CoV-2 induced an overall increase in mitochondrial networks, with significant increase in summed branch length mean values at 6 (34 and 33% increase for MOIs 0.01 and 0.1, respectively) and 24 hpi (38 and 45% increase for MOIs 0.01 and 0.1, respectively). Mitochondrial morphological analyses were further assessed by TEM (Fig. 5B) and we found that infected HBMECs displayed larger, swollen mitochondria, with reduced cristae and to some extent associated to multivesicular bodies. Moreover, MOI 0.1-infected cultures displayed 356 mitochondria/mm^2, while Mock-infected cultures had 266 mitochondria/mm^2 ($p < 0.05$), which corresponded to a 33% increase (Fig. 5D).

Since changes in mitochondrial networks could be influenced by abnormal fission or fusion events (Giacomello et al., 2020), we evaluated expression of markers of such processes. TOMM20, used to determine mitochondrial networks by confocal microscopy and MiNA analysis (Fig. 5A and C), had a 4-fold increase in its mRNA level ($p > 0.05$) in MOI 0.01-infected cells. However, no changes were detected in

TOMM20 protein levels by western blotting (Fig. 5E). We then assessed the expression of mitochondrial fission-related genes. Fis1 and Drp1 mRNA were significantly increased by 4-fold and 3-fold, respectively at 24 hpi in HBMECs infected with the MOI 0.01, which did not translate to changes in Fis1 and Drp1 protein content (Fig. 5E). Drp1 phosphorylation at serine 616 (Drpi1$^{S616)}$ residue, which is responsible for directing to mitochondrial fission (Han et al., 2020), was not altered in SARS-CoV-2-infected cultures. Mitochondrial Fission Factor (MFF) showed a 0.16-fold reduction induced by MOI 0.1 at 24 hpi, that also did not reflect into altered protein expression. However, Mitofusin-2 (Mfn2) mRNA levels showed a 4-fold increase by MOI 0.01 at 24 hpi (p = 0.02), while Mfn2 protein levels were increased by 1.5-fold in MOI 0.1-infected cultures as compared to Mock (Fig. 5E).

Discussion

Neurological consequences of COVID-19 still pose a relevant puzzle to medical and scientific community. Since its first cases, CNS invasion has been described (Paterson et al., 2020; Sanchez et al., 2021) but the routes and mechanisms by which SARS-CoV-2 gains entry to brain parenchyma remain allusive (Brann et al., 2020). In the present study we have investigated the molecular indices of Neuro-COVID-19 as they are related to brain endothelial cells forming the BBB. Despite our previous observation that primary HBMECs express several receptors for the virus (Torices et al., 2021), we found little to no indication of productive viral replication in the supernatants of HBMECs which is in accordance with previous reports that described that several endothelial cell types are not permissive for SARS-CoV-2 productive infection (McCracken et al., 2021; Nascimento Conde et al., 2021). Krasemann et al., (2022) observed infection of iPS-derived HBMECs but only at MOIs 10 and 100, which are unlikely to have pathological significance.

Exposure to SARS-CoV-2 led to augmentation of ACE2 and TMPRSS2 expression, which is consistent with our previous observations, in which HBMECs were exposed to the S1 subunit of Spike protein (Torices et al., 2021). Despite the apparent lack of productive infection, SARS-CoV-2 induced apoptotic death of HBMECs in similar levels as compared to Vero epithelial cells and to elsewhere described in the literature (Heuberger et al., 2021). In fact, HBMECs have been shown to undergo apoptotic cell death in response to viral infections, including Dengue (Meuren et al., 2021) and Zika (Leda et al., 2019; Mladinich et al., 2021) viruses, followed or not by changes in BBB permeability. These results suggest that interaction of host cells with viral surface proteins may be sufficient to trigger cellular apoptosis induction even in the absence of productive infection.

Tight junction proteins have a crucial role on maintaining BBB integrity and its selective paracellular permeability (reviewed by Takata et al., 2021). In our study, SARS-CoV-2-infected Vero E6 cells showed a marked disorganization of paracellular tight junctions, as shown by ZO-1 immunostaining. Previous studies described that treatment of HBMECs in 2D or 3D cultures with the S1 subunit Spike1 protein led to mislocalization of ZO-1, concomitantly with cytokine secretion (Buzhdygan et al., 2020; DeOre et al., 2021). Not only ZO-1 (Hao et al., 2020), but also β-catenin, cadherin-5 and occludin junctional proteins have recently been shown to be affected by SARS-CoV-2 proteins in HUVECs (Rauti et al., 2021). ZO-1 possesses a PDZ domain, which is responsible for binding and interaction with other proteins (Saras & Heldin, 1996; Giepmans & Moolenaar, 1998). Interestingly, ACE2 possesses a PDZ-binding domain

(Dasgupta & Bandyopadhyay, 2021; Caillet-Saguy & Wolff, 2021), and it has been suggested that epitopes of viral proteins, such as 1–60: M1Lys60 and 241–300: Ala240-Glu300 could directly bind to ZO-1 and VCAM-1 PDZ domains, thus suggesting a possible alternative route of CNS entry. We found ZO-1 and claudin-5 protein levels to be increased after 24 h of infection in HBMECs and this increase is consistent with what our group recently demonstrated with S1 treatment (Torices et al., 2021). Whether ZO-1 increase can be directly related to BBB permeability may vary among experimental models and infectious agents. We have described that the Honduras isolate of Zika virus selectively up-regulates ZO-1 expression *in vitro*, while BBB permeability was increased *in vivo* (Leda et al., 2019). In fact, proper BBB functioning relies on the combined expression and localization of ZO-1, -2 and − 3, claudin-5 and occludin (Feng et al., 2018). Direct infection with higher MOIs of SARS-CoV-2 or treatment with plasma from COVID-19 patients failed to induce significant increases in permeability in BMECs *in vitro* (Constant et al., 2021). Conversely, using the K18 mouse model and hamster infection, Zhang et al. (2021) showed that SARS-CoV-2 effectively infects and replicates in HBMECs, but leads to no change in BBB permeability and TJ proteins. Interestingly, a massive inoculation of iPS-derived HBMECs (MOIs 10 and 100), showed active viral replication, whereas MOIs 0.1 and 1 described infectivity near to 0.6% cells, which is similar to what we observed herein (Krasemann et al., 2022).

Following the initial characterization of infectivity profile in HBMECs, we sought to characterize the transcriptomic landscape of SARS-CoV-2 infection in BBB-forming cells. We performed RNA-Seq analyses of SARS-CoV-2-infected cultures at 6 and 24 hpi, with MOIs 0.1 and 0.01. Due to the minimal change in the overall host cell transcriptome with most of the experimental conditions used in this study, we focused our subsequent analyses to the MOI 0.1 infection at 24 hpi. The majority of the significantly up-regulated genes corresponded to known endothelial activation pathways, including CXCL1, -2, -3 and CCL20, PTX3, ICAM1 and TNF. Interestingly, the overexpression of the LTB-TNF-RELB ensemble by SARS-CoV-2, provided evidence that activation of the non-canonical NF-κB pathway activation may be taking place. NF-κB is a family of transcription factors that can be activated by several ligands and activates the expression of proinflammatory cytokines and chemokines (Sun et al., 2012). Interestingly, the main protease of SARS-CoV-2 (M^pro) cleaves a member of the NF-κB family, NEMO, which in turn leads to HBMEC cell death *in vitro* and *in vivo* (Wenzel et al., 2021). RELB can form heterodimers with p50/p105, p52/p100 and p65 (Shih et al., 2012; reviewed by Mockenhaupt et al., 2021), but can also bind to sirtuin1 to direct epigenetic silencing of inflammatory gene expression (Chen et al., 2009; Liu et al., 2011). In fact, among KEGG pathways enriched in our datasets, we found ribosomal structure and function as possible candidates for epigenetic regulation induced by SARS-CoV-2. These observations suggest that host epigenetic factors may be key for the outcome of COVID-19 and/or long COVID-19. Indeed, the promoters of the genes involved in inflammation, including NF-κB, can be demethylated, thereby resulting in an increased expression of interferons (IFNs), possibly leading to "cytokine storm" (Coit et al., 2016). The expression of IL-6, another important player in the so-called cytokine storm occurring in the most severe COVID-19 patients, was also significantly increased in infected HBMEC and it is known to be modulated by methylation of its promoter. It was also observed that oxidative stress induced by viral infections, including SARS-CoV-2 infection, can inhibit the maintenance of DNA methyltransferase DNMT1, thereby

aggravating the DNA methylation defects (Li et al., 2014; Perl, 2013; Sawalha et al., 2020). Our preliminary results (not shown) indicate that SARS-CoV-2 infection of HBMEC results in a decrease in DNA methylation, supporting a recent study of genome-wide DNA methylation analysis in peripheral blood of COVID-19 infected individuals, which identified marked epigenetic signatures, such as hypermethylation of IFN-related genes and hypomethylation of inflammatory genes (Corely et al., 2020). Such observations further suggest the involvement of epigenetic regulatory mechanisms in COVID-19 (Mantovani A & Netea, 2020).

As stated above, PTX3 was one of the main hits found in the transcriptomic analyses. Pentraxins are a superfamily of multifunctional proteins with conserved phylogeny (Daigo et al., 2014), divided into 2 groups based on their primary structure: short and long pentraxin, where c-reactive protein and PTX are examples of short and long pentraxins, respectively. PTX3 is expressed in several neural cell types (Muffley et al., 2012; Shindo et al., 2016; Freezer et al., 2017; Siqueira et al., 2018; Wesley et al., 2022) and in endothelial cells can be upregulated by inflammatory stress such as cytokine stimulation (Breviario et al., 1992). We performed a profiling of angiogenesis-related panel in the supernatants of SARS-CoV-2-infected HBMEC and confirmed that PTX3 was increased by infection. PTX3 is known to be produced in high amounts by blood vessels in vascular inflammatory conditions (Fazzini et al., 2001) and inhibits FGF2-dependent angiogenesis (Rusnati et al., 2004; Presta et al., 2018). Pathological vascularization and angiogenesis have been described as a unique comorbidity associated with SARS-CoV-2 infection in the pulmonary endothelium (Meini et al., 2020), including microvascular distortion and increased intussusceptive angiogenesis (Ackerman et al., 2020; Mentzer et al., 2022). Moreover, VEGF as well as other angiogenic-related analytes were found to be increased in COVID-19 patients (including PTX3), which correlated with disease severity (Maldonado et al., 2022). Accordingly, VEGF levels were 8% increased in the supernatants of infected HBMECs, even though *vegf* transcripts remained unaltered. It is well-known that inflammation, especially IL-6-dependent, can stimulate defective angiogenesis (Gopinathan et al., 2015) and our data further contributes to the notion that following SARS-CoV-2 infection there is an intense brain endothelial activation which leads to defective angiogenic signaling and possibly endothelial permeability. Additionally, we found HIF-1α to be greatly increased after 24 hpi. HIF-1α is a major angiogenesis inductor and is known to be up-regulated by distinct viral infections (reviewed by Reyes et al., 2020). HIF-1α is activated and translocated to the nucleus upon hypoxic conditions (Ke & Costa, 2006) and it has been shown that COVID-19 patients present massive hypoxia due to vasoconstriction and coagulopathy (Afsar et al., 2020). Interestingly, ACE2 expression is decreased in pulmonary smooth muscle cells upon HIF-1α accumulation (Zhang et al., 2020), whereas hypoxia leads to a biphasic modulation of both ACE2 and TMPRSS2 expression on brain microvascular endothelial cells (hCMEC/D3), with an initial increase at 6 h and a decrease at 48 h of hypoxic stimulus cells (Imperio et al., 2021). These observations are in accordance with our present data, that ACE2 is decreased while HIF-1α is increased at 24 hpi. Although VEGF is one of the most described downstream targets of HIF-1α activation, apoptotic cell death and IFN-stimulated gene expression are additional targets of HIF-1α activation (Reyes et al., 2020), which can also be dependent on NF-κB signaling pathway (Walmsley et al., 2005). Our data indicates that HIF-1α up-regulation can be a part of a SARS-

CoV-2-induced endothelial activation, along with cytokine/chemokine stimulation and NF-κB non-canonical activation.

Our final series of experiments focused on mitochondrial morphology and dynamics in HBMECs following SARS-CoV-2 infection. It is well known that mitochondria are gatekeepers of BBB endothelium physiology and correspond to higher cytoplasmic volume as compared to non-cerebrovascular endothelial cells (Oldendorf et al., 1977; reviewed by Parodi-Rullan et al., 2021). Moreover, mitochondrial function is important for BBB maintenance and integrity (Doll et al., 2015). We first employed a morphological/morphometrical approach to determine the mitochondrial contents and cellular distribution. Herein we demonstrated that direct exposure to SARS-CoV-2 led to a remodeling of mitochondrial networks. By using the MiNA plugin, we verified that infected HBMECs had increased mitochondrial footprint, as an estimation of overall TOMM20 pixel signal. Recent reports have also shown an effect of SARS-CoV-2 and COVID-19 on mitochondrial biology: monocytes isolated from COVID-19 patients display reduced mitochondrial membrane potential and SARS-CoV-2 viral load was positively correlated with generation of ROS (Romão et al., 2022). Importantly, endothelial cells exposed to SARS-CoV-2 Spike1 protein showed decreased tubular and increased fragmented mitochondrial networks *in vitro*, which was accompanied by a decrease in oxygen consumption rate and increase extracellular acidification rate (Lei et al., 2021). Confirming observation was recently described by Domizio et al. (2022), in which pulmonary endothelial cells in a lung-on-a-chip infection model displayed increased mitochondrial networks. Similarly, we demonstrated that mitochondrial networks were increased, as determined by summed branch length analyses, which indicates that SARS-CoV-2-infected HBMECs had longer mitochondrial ramifications. Changes in endothelial mito-morphology are well described in several models of inflammatory diseases and/or aging (Burns et al., 1979; Jendrach et al., 2005; Forrester et al., 2020) and are correlated with abnormalities in mitochondrial quality control system, which in turn can lead to increased ROS production. Mitochondrial quality control encompasses biogenesis, fission, fusion and mitophagy processes, which are essential for its biology and function. We analyzed markers of fusion and fission processes in SARS-CoV-2-infected cultures and determined that while MOI 0.01 led to an increase in fission-related gene expression (Fis1 and Drp1), this effect was not observed in protein levels or phosphorylation. However, mitofusin2 protein contents were found to be increased in MOI 0.1-infected cultures, which could explain the increased values in branch lengths. Moreover, we found mitochondria associated to some extent to multivesicular bodies, which has also been described as another pathway for mitochondrial quality control (Sugiura et al., 2014; Picca et al., 2020). Interestingly, several reports have linked NF-κB mediated inflammation with mitochondrial responses (Nakahira et al., 2011; Zhou et al., 2016; Zhong et al., 2016; Liu et al., 2018), which could indicate that in fact mitochondrial remodeling observed in infected HBMECs could be due to (or lead to) SARS-CoV-2-induced inflammatory response.

Conclusions

Despite no active replication or signs of massive infection, SARS-CoV-2 affects expression of ACE2 and TMPRSS2 in brain endothelial cells and leads to a proinflammatory activation, possibly mediated by NF-

κB non-canonical pathway activation. These events would result in mitochondrial and tight junction remodeling and endothelial apoptosis. Taken together our data point to a relevant role of SARS-CoV-2 infection on BBB-forming endothelial cells, which could reflect important aspects of clinical observations of neurological and cerebral vascular manifestations of COVID-19.

Declarations

References

1. Otsu N. A threshold selection method from gray-level histograms. *IEEE Trans Syst Man Cybern*. 1979;9(1):62−66.
2. Valente AJ, Maddalena LA, Robb EL, Moradi F, Stuart JA. A simple ImageJ macro tool for analyzing mitochondrial network morphology in mammalian cell culture. *Acta Histochem*. 2017. Doi:10.1016/j.acthis.2017.03.001
3. Arganda-Carreras I, Fernández-González R, Muñoz-Barrutia A, Ortiz-De-Solorzano C. 3D reconstruction of histological sections: Application to mammary gland tissue. *Microsc Res Tech*. 2010. Doi:10.1002/jemt.20829
4. Lee TC, Kashyap RL, Chu CN. Building Skeleton Models via 3-D Medial Surface Axis Thinning Algorithms. *CVGIP Graph Model Image Process*. 1994. Doi:10.1006/cgip.1994.1042
5. HISAT2: Kim D, Langmead B and Salzberg SL. (2015) HISAT: a fast spliced aligner with low memory requirements. Nature Methods. http://ccb.jhu.edu/software/hisat2/index.shtml

6. featureCounts: Liao Y, Smyth GK and Shi W (2014). featureCounts: an efficient general purpose program for assigning sequence reads to genomic features. Bioinformatics, 30(7):923–30. http://bioinf.wehi.edu.au/featureCounts/

7. Benjamini, Y. & Hochberg, Y. (1995) Controlling the False Discover Rate: A Practical and Powerful Approach to Multiple Testing. Journal of the Royal Statistical Society. Series B. 57: 289–300

8. https://www.cdc.gov › covid-data

9. https://data.cdc.gov › Case-Surveillance ›

10. Coronaviridae Study Group of the International Committee on Taxonomy of Viruses. The species Severe acute respiratory syndrome-related coronavirus: classifying 2019-nCoV and naming it SARS-CoV-2. Nat Microbiol 5, 536–544, 2020.

11. Zhu N, Zhang D, Wang W, Li X, Yang B, Song J, Zhao X, Huang B, Shi W, Lu R, Niu P, Zhan F, Ma X, Wang D, Xu W, Wu G, Gao GF, Tan W. China Novel Coronavirus Investigating and Research Team. A novel coronavirus from patients with pneumonia in China N Engl J Med 382, 727–733, 2020.

12. Ni J, Xiao S, Li X, Sun L. ACE gene missense mutation in a case with early-onset, rapid progressing dementia. Gen Psychiatr 32, e100028, 2019.

13. Torices S, Cabrera R, Stangis M, Naranjo O, Fattakhov N, Teglas T, Adesse D, Toborek M. Expression of SARS-CoV-2-related receptors in cells of the neurovascular unit: implications for HIV-1 infection. J Neuroinflammation 18, 67, 2021.

14. Torices, S., Cabrera, R., Stangis, M., Naranjo, O., Fattakhov, N., Teglas, T., Adesse, D., & Toborek, M. (2021). Expression of SARS-CoV-2-related receptors in cells of the neurovascular unit: implications for HIV-1 infection. Journal of neuroinflammation, 18(1), 167. https://doi.org/10.1186/s12974-021-02210-2

15. Hoffmann M, Kleine-Weber H, Schroeder S, Krüger N, Herrler T, Erichsen S, Schiergens TS, Herrler G, Wu NH, Nitsche A, Müller MA, Drosten C, Pöhlmann S. SARS-CoV-2 Cell Entry Depends on ACE2 and TMPRSS2 and Is Blocked by a Clinically Proven Protease Inhibitor. Cell 181, 271–280 e8, 2020.

16. Zhou P, Yang XL, Wang XG, Hu B, Zhang L, Zhang W, Si HR, Zhu Y, Li B, Huang CL, Chen HD, Chen J, Luo Y, Guo H, Jiang RD, Liu MQ, Chen Y, Shen XR, Wang X, Zheng XS, Zhao K, Chen QJ, Deng F, Liu LL, Yan B, Zhan FX, Wang YY, Xiao GF, Shi ZL. A pneumonia outbreak associated with a new coronavirus of probable bat origin. Nature 579, 270–273, 2020.

17. Shulla A, Heald-Sargent T, Subramanya G, Zhao J, Perlman S, Gallagher T. A transmembrane serine protease is linked to the severe acute respiratory syndrome coronavirus receptor and activates virus entry. J Virol 85, 873–882, 2011.

18. Zipeto D, Palmeira JDF, Arganaraz GA, Arganaraz ER. ACE2/ADAM17/TMPRSS2 Interplay May Be the Main Risk Factor for COVID-19. Front Immunol 11, 576745, 2020.

19. Schreiber B, Patel A, Verma A. Shedding Light on COVID-19: ADAM17 the Missing Link? Am J Ther. 2020.

20. Solerte SB, Di Sabatino A, Galli M, Fiorina P. Dipeptidyl peptidase-4 (DPP4) inhibition in COVID-19. Acta Diabetol 57, 779–783, 2020.

21. Bassendine MF, Bridge SH, McCaughan GW, Gorrell MD. COVID-19 and comorbidities: A role for dipeptidyl peptidase 4 (DPP4) in disease severity? J Diabetes 12, 649–658, 2020.

22. Cui C, Huang C, Zhou W, Ji X, Zhang F, Wang L, Zhou Y, Cui Q. AGTR2, one possible novel key gene for the entry of SARS-CoV-2 into human cells. IEEE/ACM Trans Comput Biol Bioinform. 2020.

23. de Sousa AK, Magalhaes DA, Ferreira JDS, Barbosa A. SARS-CoV-2-mediated encephalitis: Role of AT2R receptors in the blood-brain barrier. Med Hypotheses 144, 110213, 2020.

24. Wang K, Chen W, Zhang Z, Deng Y, Lian JQ, Du P, Wei D, Zhang Y, Sun XX, Gong L, Yang X, He L, Zhang L, Yang Z, Geng JJ, Chen R, Zhang H, Wang B, Zhu YM, Nan G, Jiang JL, Li L, Wu J, Lin P, Huang W, Xie L, Zheng ZH, Zhang K, Miao JL, Cui HY, Huang M, Zhang J, Fu L, Yang XM, Zhao Z, Sun S, Gu H, Wang Z, Wang CF, Lu Y, Liu YY, Wang QY, Bian H, Zhu P, Chen ZN. CD147-spike protein is a novel route for SARS-CoV-2 infection to host cells. Signal Transduct Target Ther 5, 283, 2020.

25. Qiao J, Li W, Bao J, Peng Q, Wen D, Wang J, Sun B. The expression of SARS-CoV-2 receptor ACE2 and CD147, and protease TMPRSS2 in human and mouse brain cells and mouse brain tissues. Biochem Biophys Res Commun 533, 867–871, 2020.

26. Qi F, Qian S, Zhang S, Zhang Z. Single cell RNA sequencing of 13 human tissues identify cell types and receptors of human coronaviruses. Biochem Biophys Res Commun 526, 135–140, 2020.

27. Padmanabhan P, Desikan R, Dixit NM. Targeting TMPRSS2 and Cathepsin B/L together may be synergistic against SARS-CoV-2 infection. PloS Comput Biol 16, e1008461, 2020.

28. Istlfl IE, SihoGlu Tepe A, SarikUrkc UC, Tepe B. Interaction of certain monoterpenoid hydrocarbons with the receptor binding domain of 2019 novel coronavirus (2019-nCoV), transmembrane serine protease 2 (TMPRSS2), cathepsin B, and cathepsin L (CatB/L) and their pharmacokinetic properties. Turk J Biol 44, 242–264, 2020.

29. Ellul MA, Benjamin L, Singh B, Lant S, Michael BD, Easton A, Kneen R, Defres S, Sejvar J, Solomon T. Neurological associations of COVID-19. Lancet Neurol 19, 767–783, 2020.

30. Mao L, Jin H, Wang M, Hu Y, Chen S, He Q, Chang J, Hong C, Zhou Y, Wang D, Miao X, Li Y, Hu B. Neurologic Manifestations of Hospitalized Patients With Coronavirus Disease 2019 in Wuhan, China. JAMA Neurol 77, 683–690, 2020.

31. Solomon IH, Normandin E, Bhattacharyya S, Mukerji SS, Keller K, Ali AS, Adams G, Hornick JL, Padera RF Jr, Sabeti P. Neuropathological Features of Covid-19. N Engl J Med 383, 989–992, 2020.

32. Virhammar J, Kumlien E, Fällmar D, Frithiof R, Jackmann S, Sköld MK, Kadir M, Frick J, Lindeberg J, Olivero-Reinius H, Ryttlefors M, Cunningham JL, Wikström J, Grabowska A, Bondeson K, Bergquist J, Zetterberg H, Rostami E.Acute necrotizing encephalopathy with SARS-CoV-2 RNA confirmed in cerebrospinal fluid. Neurology 95, 445–449, 2020.

33. Baig AM, Khaleeq A, Ali U, Syeda H. Evidence of the COVID-19 Virus Targeting the CNS: Tissue Distribution, Host-Virus Interaction, and Proposed Neurotropic Mechanisms. ACS Chem Neurosci11, 995–998, 2020.

34. Li Y, Li M, Wang M, Zhou Y, Chang J, Xian Y, Wang D, Mao L, Jin H, Hu B. 2020a. Acute cerebrovascular disease following COVID-19: a single center, retrospective, observational study.

Stroke Vasc Neurol 5, 279–284,.

35. Li Z, Liu T, Yang N, Han D, Mi X, Li Y, Liu K, Vuylsteke A, Xiang H, Guo X. 2020b Neurological manifestations of patients with COVID-19: potential routes of SARS-CoV-2 neuroinvasion from the periphery to the brain. Front Med 14, 533–541,.

36. Briguglio M, Bona A, Porta M, Dell'Osso B, Pregliasco FE, Banfi G. Disentangling the Hypothesis of Host Dysosmia and SARS-CoV-2: The Bait Symptom That Hides Neglected Neurophysiological Routes. Front Physiol 11, 671, 2020.

37. Alam SB, Willows S, Kulka M, Sandhu JK.Severe acute respiratory syndrome coronavirus 2 may be an underappreciated pathogen of the central nervous system. Eur J Neurol 27, 2348–2360, 2020.

38. Achar A, Ghosh C. COVID-19-Associated Neurological Disorders: The Potential Route of CNS Invasion and Blood-Brain Relevance. Cells 9, 2360, 2020.

39. Abbott NJ. Dynamics of CNS barriers: evolution, differentiation, and modulation. Cell Mol Neurobiol 25, 5–23, 2005.

40. Buzhdygan TP, DeOre BJ, Baldwin-Leclair A, Bullock TA, McGary HM, Khan JA, Razmpour R, Hale JF, Galie PA, Potula R, Andrews AM, Ramirez SH. The SARS-CoV-2 spike protein alters barrier function in 2D static and 3D microfluidic in-vitro models of the human blood-brain barrier. Neurobiol Dis 146, 105131, 2020.

41. Stins, M. F., Badger, J., & Sik Kim, K. (2001). Bacterial invasion and transcytosis in transfected human brain microvascular endothelial cells. Microbial pathogenesis, 30(1), 19–28. https://doi.org/10.1006/mpat.2000.0406

42. https://.1

43. Matos AR, Caetano BC, de Almeida Filho JL, Martins JSCC, de Oliveira MGP, Sousa TdC, Horta MAP, Siqueira MM and Fernandez JH (2022) Identification of Hypericin as a Candidate Repurposed Therapeutic Agent for COVID-19 and Its Potential Anti-SARS-CoV-2 Activity. Front. Microbiol. 13:828984. Doi: 10.3389/fmicb.2022.828984

44. Terryn, C., M. Sellami, C. Fichel, M. D. Diebold, S. Gangloff, R. Le Naour, M. Polette, e J. M. Zahm. 2013. "Rapid method of quantification of tight-junction organization using image analysis". Cytometry A 83 (2): 235–41. https://doi.org/10.1002/cyto.a.22239.

45. Jiang, M., Kolehmainen, P., Kakkola, L., Maljanen, S., Melén, K., Smura, T., Julkunen, I., & Österlund, P. (2021). SARS-CoV-2 Isolates Show Impaired Replication in Human Immune Cells but Differential Ability to Replicate and Induce Innate Immunity in Lung Epithelial Cells. Microbiology spectrum, 9(1), e0077421. https://doi.org/10.1128/Spectrum.00774-21

46. Mockenhaupt, K., Gonsiewski, A., & Kordula, T. (2021). RelB and Neuroinflammation. Cells, 10(7), 1609. https://doi.org/10.3390/cells10071609

47. Presta M, Foglio E, Churruca Schuind A, Ronca R. Long Pentraxin-3 Modulates the Angiogenic Activity of Fibroblast Growth Factor-2. Front Immunol. 2018 Oct 8;9:2327. Doi: 10.3389/fimmu.2018.02327. PMID: 30349543; PMCID: PMC6187966.

48. Estato, V., Stipursky, J., Gomes, F., Mergener, T. C., Frazão-Teixeira, E., Allodi, S., Tibiriçá, E., Barbosa, H. S., & Adesse, D. (2018). The Neurotropic Parasite Toxoplasma gondii Induces Sustained Neuroinflammation with Microvascular Dysfunction in Infected Mice. The American journal of pathology, 188(11), 2674–2687. https://doi.org/10.1016/j.ajpath.2018.07.007

49. Han, H., Tan, J., Wang, R., Wan, H., He, Y., Yan, X., Guo, J., Gao, Q., Li, J., Shang, S., Chen, F., Tian, R., Liu, W., Liao, L., Tang, B., & Zhang, Z. (2020). PINK1 phosphorylates Drp1S616 to regulate mitophagy-independent mitochondrial dynamics. EMBO reports, 21(8), e48686. https://doi.org/10.15252/embr.201948686

50. McCracken, I. R., Saginc, G., He, L., Huseynov, A., Daniels, A., Fletcher, S., Peghaire, C., Kalna, V., Andaloussi-Mäe, M., Muhl, L., Craig, N. M., Griffiths, S. J., Haas, J. G., Tait-Burkard, C., Lendahl, U., Birdsey, G. M., Betsholtz, C., Noseda, M., Baker, A. H., & Randi, A. M. (2021). Lack of Evidence of Angiotensin-Converting Enzyme 2 Expression and Replicative Infection by SARS-CoV-2 in Human Endothelial Cells. Circulation, 143(8), 865–868. https://doi.org/10.1161/CIRCULATIONAHA.120.052824

51. Nascimento Conde, J., Schutt, W. R., Gorbunova, E. E., & Mackow, E. R. (2020). Recombinant ACE2 Expression Is Required for SARS-CoV-2 To Infect Primary Human Endothelial Cells and Induce Inflammatory and Procoagulative Responses. mBio, 11(6), e03185-20. https://doi.org/10.1128/mBio.03185-20

52. Heuberger, J., Trimpert, J., Vladimirova, D., Goosmann, C., Lin, M., Schmuck, R., Mollenkopf, H. J., Brinkmann, V., Tacke, F., Osterrieder, N., & Sigal, M. (2021). Epithelial response to IFN-γ promotes SARS-CoV-2 infection. EMBO molecular medicine, 13(4), e13191. https://doi.org/10.15252/emmm.202013191

53. Meuren, L. M., Prestes, E. B., Papa, M. P., de Carvalho, L., Mustafá, Y. M., da Costa, L. S., Da Poian, A. T., Bozza, M. T., & Arruda, L. B. (2022). Infection of Endothelial Cells by Dengue Virus Induces ROS Production by Different Sources Affecting Virus Replication, Cellular Activation, Death and Vascular Permeability. Frontiers in immunology, 13, 810376. https://doi.org/10.3389/fimmu.2022.810376

54. Leda, A. R., Bertrand, L., Andras, I. E., El-Hage, N., Nair, M., & Toborek, M. (2019). Selective Disruption of the Blood-Brain Barrier by Zika Virus. Frontiers in microbiology, 10, 2158. https://doi.org/10.3389/fmicb.2019.02158

55. Mladinich, M. C., Conde, J. N., Schutt, W. R., Sohn, S. Y., & Mackow, E. R. (2021). Blockade of Autocrine CCL5 Responses Inhibits Zika Virus Persistence and Spread in Human Brain Microvascular Endothelial Cells. mBio, 12(4), e0196221. https://doi.org/10.1128/mBio.01962-21

56. DeOre, B. J., Tran, K. A., Andrews, A. M., Ramirez, S. H., & Galie, P. A. (2021). SARS-CoV-2 Spike Protein Disrupts Blood-Brain Barrier Integrity via RhoA Activation. Journal of neuroimmune pharmacology: the official journal of the Society on NeuroImmune Pharmacology, 16(4), 722–728. https://doi.org/10.1007/s11481-021-10029-0

57. Hao, S., Ning, K., Kuz, C. A., Vorhies, K., Yan, Z., & Qiu, J. (2020). Long-Term Modeling of SARS-CoV-2 Infection of In Vitro Cultured Polarized Human Airway Epithelium. mBio, 11(6), e02852-20.

https://doi.org/10.1128/mBio.02852-20

58. Rauti, R., Shahoha, M., Leichtmann-Bardoogo, Y., Nasser, R., Paz, E., Tamir, R., Miller, V., Babich, T., Shaked, K., Ehrlich, A., Ioannidis, K., Nahmias, Y., Sharan, R., Ashery, U., & Maoz, B. M. (2021). Effect of SARS-CoV-2 proteins on vascular permeability. eLife, 10, e69314. https://doi.org/10.7554/eLife.69314

59. Dasgupta, S., & Bandyopadhyay, M. (2021). Molecular docking of SARS-COV-2 Spike epitope sequences identifies heterodimeric peptide-protein complex formation with human Zo-1, TLR8 and brain specific glial proteins. Medical hypotheses, 157, 110706. https://doi.org/10.1016/j.mehy.2021.110706

60. Caillet-Saguy, C., & Wolff, N. (2021). PDZ-Containing Proteins Targeted by the ACE2 Receptor. Viruses, 13(11), 2281. https://doi.org/10.3390/v13112281

61. Feng, S., Zou, L., Wang, H., He, R., Liu, K., & Zhu, H. (2018). RhoA/ROCK-2 Pathway Inhibition and Tight Junction Protein Upregulation by Catalpol Suppresses Lipopolysaccaride-Induced Disruption of Blood-Brain Barrier Permeability. Molecules (Basel, Switzerland), 23(9), 2371. https://doi.org/10.3390/molecules23092371

62. Constant, O., Barthelemy, J., Bolloré, K., Tuaillon, E., Gosselet, F., Chable-Bessia, C., Merida, P., Muriaux, D., Van de Perre, P., Salinas, S., & Simonin, Y. (2021). SARS-CoV-2 Poorly Replicates in Cells of the Human Blood-Brain Barrier Without Associated Deleterious Effects. Frontiers in immunology, 12, 697329. https://doi.org/10.3389/fimmu.2021.697329

63. Zhang, L., Zhou, L., Bao, L., Liu, J., Zhu, H., Lv, Q., Liu, R., Chen, W., Tong, W.,Wei, Q., Xu, Y., Deng, W., Gao, H., Xue, J., Song, Z., Yu, P., Han, Y., Zhang, Y.,Sun, X., Yu, X., … Qin, C. (2021). SARS-CoV-2 crosses the blood-brain barrier accompanied with basement membrane disruption without tight junctions alteration. Signal transduction and targeted therapy, 6(1), 337. https://doi.org/10.1038/s41392-021-00719-9

64. Krasemann, S., Haferkamp, U., Pfefferle, S., Woo, M. S., Heinrich, F., Schweizer,M., Appelt-Menzel, A., Cubukova, A., Barenberg, J., Leu, J., Hartmann, K., Thies,E., Littau, J. L., Sepulveda-Falla, D., Zhang, L., Ton, K., Liang, Y., Matschke, J.,Ricklefs, F., Sauvigny, T., … Pless, O. (2022). The blood-brain barrier is dysregulated in COVID-19 and serves as a CNS entry route for SARS-CoV-2. Stem cell reports, 17(2),307–320. https://doi.org/10.1016/j.stemcr.2021.12.011

65. Sun S. C. (2012). The noncanonical NF-κB pathway. Immunological reviews, 246(1), 125–140. https://doi.org/10.1111/j.1600-065X.2011.01088.x

66. Wenzel, J., Lampe, J., Müller-Fielitz, H., Schuster, R., Zille, M., Müller, K., Krohn,M., Körbelin, J., Zhang, L., Özorhan, Ü., Neve, V., Wagner, J., Bojkova, D., Shumliakivska,M., Jiang, Y., Fähnrich, A., Ott, F., Sencio, V., Robil, C., Pfefferle, S., … Schwaninger,M. (2021). The SARS-CoV-2 main protease Mpro causes microvascular brain pathology by cleaving NEMO in brain endothelial cells. Nature neuroscience, 24(11), 1522–1533.https://doi.org/10.1038/s41593-021-00926-1

67. Mockenhaupt, K., Gonsiewski, A., & Kordula, T. (2021). RelB and Neuroinflammation. Cells, 10(7), 1609. https://doi.org/10.3390/cells10071609

68. Shih, V. F., Davis-Turak, J., Macal, M., Huang, J. Q., Ponomarenko, J., Kearns, J. D., Yu, T., Fagerlund, R., Asagiri, M., Zuniga, E. I., & Hoffmann, A. (2012). Control of RelB during dendritic cell activation integrates canonical and noncanonical NF-κB pathways. Nature immunology, 13(12), 1162–1170. https://doi.org/10.1038/ni.2446

69. Chen, X.; El Gazzar, M.; Yoza, B.K.; McCall, C.E. The NF-κB factor RelB and histone H3 lysine methyltransferase G9a directly interact to generate epigenetic silencing in endotoxin tolerance. J. Biol. Chem. 2009, 284, 27857–27865.

70. Liu, T.F.; Yoza, B.K.; El Gazzar, M.; Vachharajani, V.T.; McCall, C.E. NAD+-dependent SIRT1 deacetylase participates in epigenetic reprogramming during endotoxin tolerance. J. Biol. Chem. 2011, 286, 9856–9864.

71. Coit P, De Lott LB, Nan B, Elner VM, Sawalha AH. DNA methylation analysis of the temporal artery microenvironment in giant cell arteritis. Ann Rheum Dis 75, 1196–1202, 2016

72. Li Y, Gorelik G, Strickland FM, Richardson BC. Oxidative stress, T cell DNA methylation, and lupus. Arthritis Rheumatol 66, 1574–1582, 2014.

73. Sawalha AH, Zhao M, Coit P, Lu Q. Epigenetic dysregulation of ACE2 and interferon-regulated genes might suggest increased COVID-19 susceptibility and severity in lupus patients. Clin Immunol 215, 108410, 2020.

74. Oaks Z, Perl A. Metabolic control of the epigenome in systemic Lupus erythematosus. Autoimmunity 47, 256–264, 2014.

75. Mantovani A, Netea MG. Trained Innate Immunity, Epigenetics, and Covid-19. N Engl J Med 383, 1078–1080, 2020.

76. Ihezie, S. A., Mathew, I. E., McBride, D. W., Dienel, A., Blackburn, S. L., & Thankamani Pandit, P. K. (2021). Epigenetics in blood-brain barrier disruption. Fluids and barriers of the CNS, 18(1), 17. https://doi.org/10.1186/s12987-021-00250-7

77. Daigo, K., Mantovani, A., & Bottazzi, B. (2014). The yin-yang of long pentraxin PTX3 in inflammation and immunity. Immunology letters, 161(1), 38–43. https://doi.org/10.1016/j.imlet.2014.04.012

78. Muffley, L. A., Pan, S. C., Smith, A. N., Ga, M., Hocking, A. M., & Gibran, N. S. (2012). Differentiation state determines neural effects on microvascular endothelial cells. Experimental cell research, 318(16), 2085–2093. https://doi.org/10.1016/j.yexcr.2012.06.002

79. Freese, C., Hanada, S., Fallier-Becker, P., Kirkpatrick, C. J., & Unger, R. E. (2017). Identification of neuronal and angiogenic growth factors in an in vitro blood-brain barrier model system: Relevance in barrier integrity and tight junction formation and complexity. Microvascular research, 111, 1–11. https://doi.org/10.1016/j.mvr.2016.12.001

80. Shindo, A., Maki, T., Mandeville, E. T., Liang, A. C., Egawa, N., Itoh, K., Itoh, N., Borlongan, M., Holder, J. C., Chuang, T. T., McNeish, J. D., Tomimoto, H., Lok, J., Lo, E. H., & Arai, K. (2016). Astrocyte-Derived Pentraxin 3 Supports Blood-Brain Barrier Integrity Under Acute Phase of Stroke. Stroke, 47(4), 1094–1100. https://doi.org/10.1161/STROKEAHA.115.012133

81. Wesley, U. V., Sutton, I., Clark, P. A., Cunningham, K., Larrain, C., Kuo, J. S., & Dempsey, R. J. (2022). Enhanced expression of pentraxin-3 in glioblastoma cells correlates with increased invasion and IL8-VEGF signaling axis. Brain research, 1776, 147752. https://doi.org/10.1016/j.brainres.2021.147752

82. Siqueira, M., Francis, D., Gisbert, D., Gomes, F., & Stipursky, J. (2018). Radial Glia Cells Control Angiogenesis in the Developing Cerebral Cortex Through TGF-β1 Signaling. Molecular neurobiology, 55(5), 3660–3675. https://doi.org/10.1007/s12035-017-0557-8

83. Breviario, F., d'Aniello, E. M., Golay, J., Peri, G., Bottazzi, B., Bairoch, A., Saccone, S., Marzella, R., Predazzi, V., & Rocchi, M. (1992). Interleukin-1-inducible genes in endothelial cells. Cloning of a new gene related to C-reactive protein and serum amyloid P component. The Journal of biological chemistry, 267(31), 22190–22197.

84. Fazzini, F., Peri, G., Doni, A., Dell'Antonio, G., Dal Cin, E., Bozzolo, E., D'Auria, F., Praderio, L., Ciboddo, G., Sabbadini, M. G., Manfredi, A. A., Mantovani, A., & Querini, P. R. (2001). PTX3 in small-vessel vasculitides: an independent indicator of disease activity produced at sites of inflammation. Arthritis and rheumatism, 44(12), 2841–2850. https://doi.org/10.1002/1529-0131(200112)44:12<2841::aid-art472>3.0.co;2-6

85. Rusnati, M., Camozzi, M., Moroni, E., Bottazzi, B., Peri, G., Indraccolo, S., Amadori, A., Mantovani, A., & Presta, M. (2004). Selective recognition of fibroblast growth factor-2 by the long pentraxin PTX3 inhibits angiogenesis. Blood, 104(1), 92–99. https://doi.org/10.1182/blood-2003-10-3433

86. Presta, M., Foglio, E., Churruca Schuind, A., & Ronca, R. (2018). Long Pentraxin-3 Modulates the Angiogenic Activity of Fibroblast Growth Factor-2. Frontiers in immunology, 9, 2327. https://doi.org/10.3389/fimmu.2018.02327

87. Meini S, Giani T, Tascini C. Intussusceptive angiogenesis in Covid-19: hypothesis on the significance and focus on the possible role of FGF2. Mol Biol Rep 47, 8301–8304, 2020.

88. Mentzer, S. J., Ackermann, M., & Jonigk, D. (2022). Endothelialitis, Microischemia, and Intussusceptive Angiogenesis in COVID-19. Cold Spring Harbor perspectives in medicine, a041157. Advance online publication. https://doi.org/10.1101/cshperspect.a041157

89. Ackermann, M., Mentzer, S. J., Kolb, M., & Jonigk, D. (2020). Inflammation and intussusceptive angiogenesis in COVID-19: everything in and out of flow. The European respiratory journal, 56(5), 2003147. https://doi.org/10.1183/13993003.03147-2020

90. Maldonado, F., Morales, D., Díaz-Papapietro, C., Valdés, C., Fernandez, C., Valls, N., Lazo, M., Espinoza, C., González, R., Gutiérrez, R., Jara, Á., Romero, C., Cerda, O., & Cáceres, M. (2022). Relationship Between Endothelial and Angiogenesis Biomarkers Envisage Mortality in a Prospective Cohort of COVID-19 Patients Requiring Respiratory Support. Frontiers in medicine, 9, 826218. https://doi.org/10.3389/fmed.2022.826218

91. Gopinathan, G., Milagre, C., Pearce, O. M., Reynolds, L. E., Hodivala-Dilke, K., Leinster, D. A., Zhong, H., Hollingsworth, R. E., Thompson, R., Whiteford, J. R., & Balkwill, F. (2015). Interleukin-6 Stimulates Defective Angiogenesis. Cancer research, 75(15), 3098–3107. https://doi.org/10.1158/0008-5472.CAN-15-1227

92. Reyes, A., Corrales, N., Gálvez, N., Bueno, S. M., Kalergis, A. M., & González, P. A. (2020). Contribution of hypoxia inducible factor-1 during viral infections. Virulence, 11(1), 1482–1500. https://doi.org/10.1080/21505594.2020.1836904

93. Ke Q, Costa M. Hypoxia-inducible factor-1 (HIF-1). Mol Pharmacol. 2006;70(5):1469–1480.

94. Afsar B, Kanbay M, Afsar RE. Hypoxia inducible factor-1 protects against COVID-19: a hypothesis. Med Hypotheses. 2020;143:109857.

95. Zhang R, Wu Y, Zhao M, et al. Role of HIF-1α in the regulation ACE and ACE2 expression in hypoxic human pulmonary artery smooth muscle cells. Am J Physiol Lung Cell Mol Physiol. 2009;297(4):L631- L640.

96. Imperio, G. E., Lye, P., Mughis, H., Hamada, H., Bloise, E., Lye, S. J., & Matthews, S. G. (2021). Hypoxia alters the expression of ACE2 and TMPRSS2 SARS-CoV-2 cell entry mediators in hCMEC/D3 brain endothelial cells. Microvascular research, 138, 104232. https://doi.org/10.1016/j.mvr.2021.104232

97. Walmsley SR, Print C, Farahi N, et al. Hypoxiainduced neutrophil survival is mediated by HIF-1αdependent NF-κB activity. J Exp Med. 2005;201 (1):105–115.

98. Parodi-Rullán, R. M., Javadov, S., & Fossati, S. (2021). Dissecting the Crosstalk between Endothelial Mitochondrial Damage, Vascular Inflammation, and Neurodegeneration in Cerebral Amyloid Angiopathy and Alzheimer's Disease. Cells, 10(11), 2903. https://doi.org/10.3390/cells10112903

99. Oldendorf, W. H., Cornford, M. E., and Brown, W. J. (1977). The large apparent work capability of the blood-brain barrier: a study of the mitochondrial content of capillary endothelial cells in brain and other tissues of the rat. Ann. Neurol. 1, 409–417. Doi: 10.1002/ana.410010502

100. Doll, D. N., Hu, H., Sun, J., Lewis, S. E., Simpkins, J. W., & Ren, X. (2015). Mitochondrial crisis in cerebrovascular endothelial cells opens the blood-brain barrier. Stroke, 46(6), 1681–1689. https://doi.org/10.1161/STROKEAHA.115.009099

101. Romão, P. R., Teixeira, P. C., Schipper, L., da Silva, I., Santana Filho, P., Júnior, L., Peres, A., Gonçalves da Fonseca, S., Chagas Monteiro, M., Lira, F. S., Andrey Cipriani Frade, M., Comerlato, J., Comerlato, C., Sant'Anna, F. H., Bessel, M., Abreu, C. M., Wendland, E. M., & Dorneles, G. P. (2022). Viral load is associated with mitochondrial dysfunction and altered monocyte phenotype in acute severe SARS-CoV-2 infection. International immunopharmacology, 108, 108697. Advance online publication. https://doi.org/10.1016/j.intimp.2022.108697

102. Lei, Y., Zhang, J., Schiavon, C. R., He, M., Chen, L., Shen, H., Zhang, Y., Yin, Q.,Cho, Y., Andrade, L., Shadel, G. S., Hepokoski, M., Lei, T., Wang, H., Zhang, J.,Yuan, J. X., Malhotra, A., Manor, U., Wang, S., Yuan, Z. Y., … Shyy, J. Y. (2021).SARS-CoV-2 Spike Protein Impairs Endothelial Function via Downregulation of ACE 2.Circulation research, 128(9), 1323–1326. https://doi.org/10.1161/CIRCRESAHA.121.318902

103. Domizio, J. D., Gulen, M. F., Saidoune, F., Thacker, V. V., Yatim, A., Sharma, K., Nass, T., Guenova, E., Schaller, M., Conrad, C., Goepfert, C., de Leval, L., Garnier, C. V., Berezowska, S., Dubois, A., Gilliet, M., & Ablasser, A. (2022). The cGAS-STING pathway drives type I IFN immunopathology in COVID-19. Nature, 603(7899), 145–151. https://doi.org/10.1038/s41586-022-04421-w

104. Forrester, S. J., Preston, K. J., Cooper, H. A., Boyer, M. J., Escoto, K. M., Poltronetti, A. J., Elliott, K. J., Kuroda, R., Miyao, M., Sesaki, H., Akiyama, T., Kimura, Y., Rizzo, V., Scalia, R., & Eguchi, S. (2020). Mitochondrial Fission Mediates Endothelial Inflammation. Hypertension (Dallas, Tex.: 1979), 76(1), 267–276. https://doi.org/10.1161/HYPERTENSIONAHA.120.14686

105. Jendrach, M., Pohl, S., Vöth, M., Kowald, A., Hammerstein, P., & Bereiter-Hahn, J. (2005). Morpho-dynamic changes of mitochondria during ageing of human endothelial cells. Mechanisms of ageing and development, 126(6–7), 813–821. https://doi.org/10.1016/j.mad.2005.03.002

106. Burns, E. M., Kruckeberg, T. W., Comerford, L. E., & Buschmann, M. T. (1979). Thinning of capillary walls and declining numbers of endothelial mitochondria in the cerebral cortex of the aging primate, Macaca nemestrina. Journal of gerontology, 34(5), 642–650. https://doi.org/10.1093/geronj/34.5.642

107. Won, J., Lee, S., Park, M., Kim, T. Y., Park, M. G., Choi, B. Y., Kim, D., Chang, H., Kim, V. N., & Lee, C. J. (2020). Development of a Laboratory-safe and Low-cost Detection Protocol for SARS-CoV-2 of the Coronavirus Disease 2019 (COVID-19). Experimental neurobiology, 29(2), 107–119. https://doi.org/10.5607/en20009

108. Zhong, Z., Umemura, A., Sanchez-Lopez, E., Liang, S., Shalapour, S., Wong, J., He, F., Boassa, D., Perkins, G., Ali, S. R., McGeough, M. D., Ellisman, M. H., Seki, E., Gustafsson, A. B., Hoffman, H. M., Diaz-Meco, M. T., Moscat, J., & Karin, M. (2016). NF-κB Restricts Inflammasome Activation via Elimination of Damaged Mitochondria. Cell, 164(5), 896–910. https://doi.org/10.1016/j.cell.2015.12.057

109. Nakahira, K., Haspel, J. A., Rathinam, V. A., Lee, S. J., Dolinay, T., Lam, H. C., Englert, J. A., Rabinovitch, M., Cernadas, M., Kim, H. P., Fitzgerald, K. A., Ryter, S. W., & Choi, A. M. (2011). Autophagy proteins regulate innate immune responses by inhibiting the release of mitochondrial DNA mediated by the NALP3 inflammasome. Nature immunology, 12(3), 222–230. https://doi.org/10.1038/ni.1980

110. Zhou, R., Yazdi, A. S., Menu, P., & Tschopp, J. (2011). A role for mitochondria in NLRP3 inflammasome activation. Nature, 469(7329), 221–225. https://doi.org/10.1038/nature09663

111. Liu, Q., Zhang, D., Hu, D., Zhou, X., & Zhou, Y. (2018). The role of mitochondria in NLRP3 inflammasome activation. Molecular immunology, 103, 115–124. https://doi.org/10.1016/j.molimm.2018.09.010

112. Giacomello, M., Pyakurel, A., Glytsou, C. et al. The cell biology of mitochondrial membrane dynamics. Nat Rev Mol Cell Biol 21, 204–224 (2020). https://doi.org/10.1038/s41580-020-0210-7.

113. Wang, K., Chen, W., Zhang, Z., Deng, Y., Lian, J. Q., Du, P., Wei, D., Zhang, Y.,Sun, X. X., Gong, L., Yang, X., He, L., Zhang, L., Yang, Z., Geng, J. J., Chen, R.,Zhang, H., Wang, B., Zhu, Y. M., Nan, G., … Chen, Z. N. (2020). CD147-spike protein is a novel route for SARS-CoV-2 infection to host cells. Signal transduction and targeted therapy, 5(1), 283. https://doi.org/10.1038/s41392-020-00426-x.

114. Won, J., Lee, S., Park, M., Kim, T. Y., Park, M. G., Choi, B. Y., Kim, D., Chang, H., Kim, V. N., & Lee, C. J. (2020). Development of a Laboratory-safe and Low-cost Detection Protocol for SARS-CoV-2 of the

Coronavirus Disease 2019 (COVID-19). Experimental neurobiology, 29(2), 107–119. https://doi.org/10.5607/en20009.

115. Corman, V. M., Landt, O., Kaiser, M., Molenkamp, R., Meijer, A., Chu, D. K., Bleicker,T., Brünink, S., Schneider, J., Schmidt, M. L., Mulders, D. G., Haagmans, B. L., van der Veer, B., van den Brink, S., Wijsman, L., Goderski, G., Romette, J. L., Ellis,J., Zambon, M., Peiris, M., … Drosten, C. (2020). Detection of 2019 novel coronavirus(2019-nCoV) by real-time RT-PCR. Euro surveillance: bulletin Europeen sur les maladies transmissibles = European communicable disease bulletin, 25(3), 2000045. https ://doi.org/10.2807/1560-7917.ES.2020.25.3.2000045.

116. Valencia Sanchez, C., Theel, E., Binnicker, M., Toledano, M., & McKeon, A. (2021). Autoimmune Encephalitis After SARS-CoV-2 Infection: Case Frequency, Findings, and Outcomes. Neurology, 97(23), e2262–e2268. https://doi.org/10.1212/WNL.0000000000012931.

117. Paterson, R. W., Brown, R. L., Benjamin, L., Nortley, R., Wiethoff, S., Bharucha,T., Jayaseelan, D. L., Kumar, G., Raftopoulos, R. E., Zambreanu, L., Vivekanandam,V., Khoo, A., Geraldes, R., Chinthapalli, K., Boyd, E., Tuzlali, H., Price, G., Christofi,G., Morrow, J., McNamara, P., … Zandi, M. S. (2020). The emerging spectrum of COVID-19 neurology: clinical, radiological and laboratory findings. Brain : a journal of neurology,143(10), 3104–3120. https ://doi.org/10.1093/brain/awaa240.

118. Brann, D. H., Tsukahara, T., Weinreb, C., Lipovsek, M., Van den Berge, K., Gong, B.,Chance, R., Macaulay, I. C., Chou, H. J., Fletcher, R. B., Das, D., Street, K., de Bezieux, H. R., Choi, Y. G., Risso, D., Dudoit, S., Purdom, E., Mill, J., Hachem,R. A., Matsunami, H., … Datta, S. R. (2020). Non-neuronal expression of SARS-CoV-2 entry genes in the olfactory system suggests mechanisms underlying COVID-19-associated anosmia. Science advances, 6(31), eabc5801. https://doi.org/10.1126/sciadv.abc5801.

119. Takata, F., Nakagawa, S., Matsumoto, J., & Dohgu, S. (2021). Blood-Brain Barrier Dysfunction Amplifies the Development of Neuroinflammation: Understanding of Cellular Events in Brain Microvascular Endothelial Cells for Prevention and Treatment of BBB Dysfunction. Frontiers in cellular neuroscience, 15, 661838. https://doi.org/10.3389/fncel.2021.661838

120. Giepmans, B. N., & Moolenaar, W. H. (1998). The gap junction protein connexin43 interacts with the second PDZ domain of the zona occludens-1 protein. Current biology: CB, 8(16), 931–934. https://doi.org/10.1016/s0960-9822(07)00375-2

121. Saras, J., & Heldin, C. H. (1996). PDZ domains bind carboxy-terminal sequences of target proteins. Trends in biochemical sciences, 21(12), 455–458. https://doi.org/10.1016/s0968-0004(96)30044-3.

122. https://covid19.who.int/

123. WHO 2022: https://www.who.int/activities/tracking-SARS-CoV-2-variants

124. Zhu, N., Zhang, D., Wang, W., Li, X., Yang, B., Song, J., Zhao, X., Huang, B., Shi, W., Lu, R., Niu, P., Zhan, F., Ma, X., Wang, D., Xu, W., Wu, G., Gao, G. F., Tan, W., & China Novel Coronavirus Investigating and Research Team (2020). A Novel Coronavirus from Patients with Pneumonia in China, 2019. The New England journal of medicine, 382(8), 727–733. https://doi.org/10.1056/NEJMoa2001017

125. https://covid.cdc.gov/covid-data-tracker/#datatracker-home

126. CDC 2020: https://data.cdc.gov/Case-Surveillance/COVID-19-Case-Surveillance-Public-Use-Data/vbim-akqf

127. WHO, 2021: https://www.who.int/publications/i/item/WHO-WPE-GIH-2021.1

128. Sugiura, A., McLelland, G. L., Fon, E. A., & McBride, H. M. (2014). A new pathway for mitochondrial quality control: mitochondrial-derived vesicles. The EMBO journal, 33(19), 2142–2156. https://doi.org/10.15252/embj.201488104

129. Picca, A., Guerra, F., Calvani, R., Coelho-Junior, H. J., Bossola, M., Landi, F., Bernabei, R., Bucci, C., & Marzetti, E. (2020). Generation and Release of Mitochondrial-Derived Vesicles in Health, Aging and Disease. Journal of clinical medicine, 9(5), 1440. https://doi.org/10.3390/jcm9051440
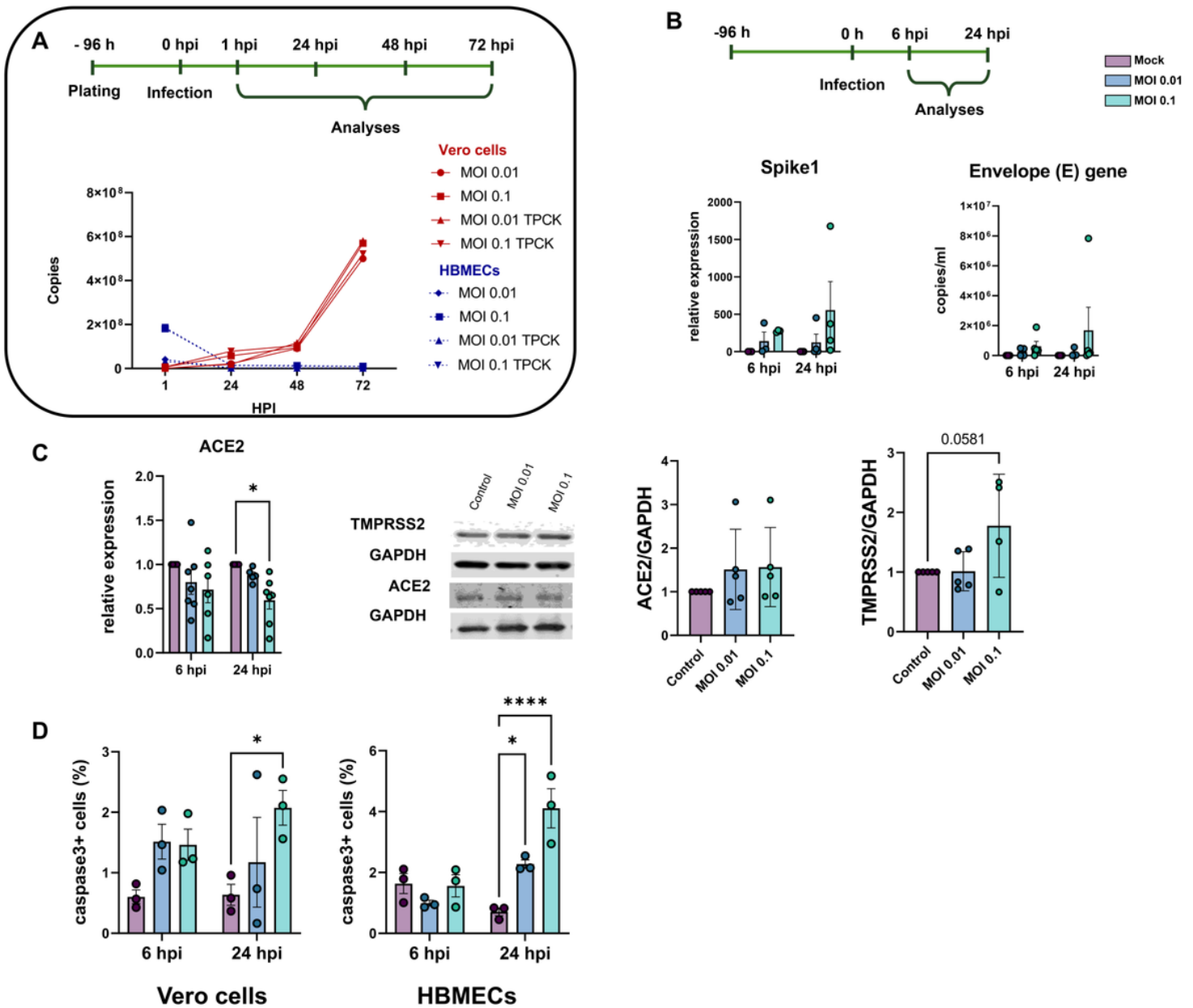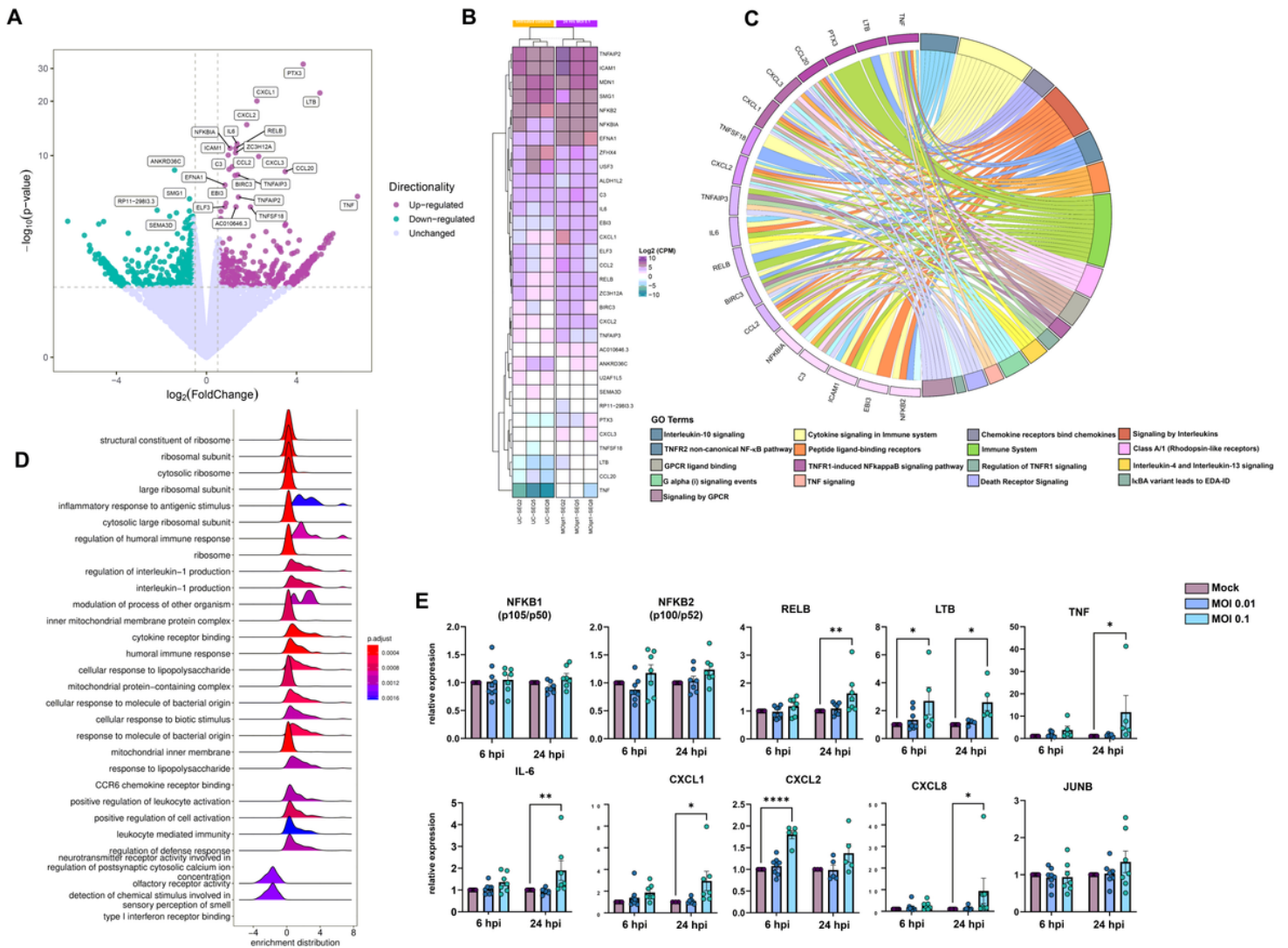
Figures

Figure 1

Characterization of infectivity profile of HBMECs by SARS-CoV-2. (**A**) HBMECs were infected with different MOIs of SARS-CoV-2 (variant D614G) and viral production and release to supernatant was analyzed by RT-qPCR for Envelope (E) gene from 0 to 72 hours post infection (hpi). As compared to Vero cells, HBMECs showed a non-productive infection. (**B**) At desired time points (6 and 24 hpi) total RNA from cultures and expression of Spike1 and E genes were analyzed by RT-qPCR. Infection with MOI 0.1 showed an increase in expression of these two transcripts at 24 hpi ($p > 0.05$). (**C**) Evaluation of SARS-CoV-2 receptors expression in infected HBMECs. ACE2 mRNA had a significant decrease at 24 hpi with the MOI 0.1, which did not translate to protein levels (right panel). TMPRSS2 had a slight increase in protein content at 24 hpi. (**D**) SARS-CoV-2 induces apoptotic cell death in Vero and HBME cells at 24 hpi as measured by cleaved caspase-3 immunostaining. *: $p < 0.05$; ****: $p < 0.0001$, Two-Way ANOVA with Bonferroni post-test of at least five independent experiments.
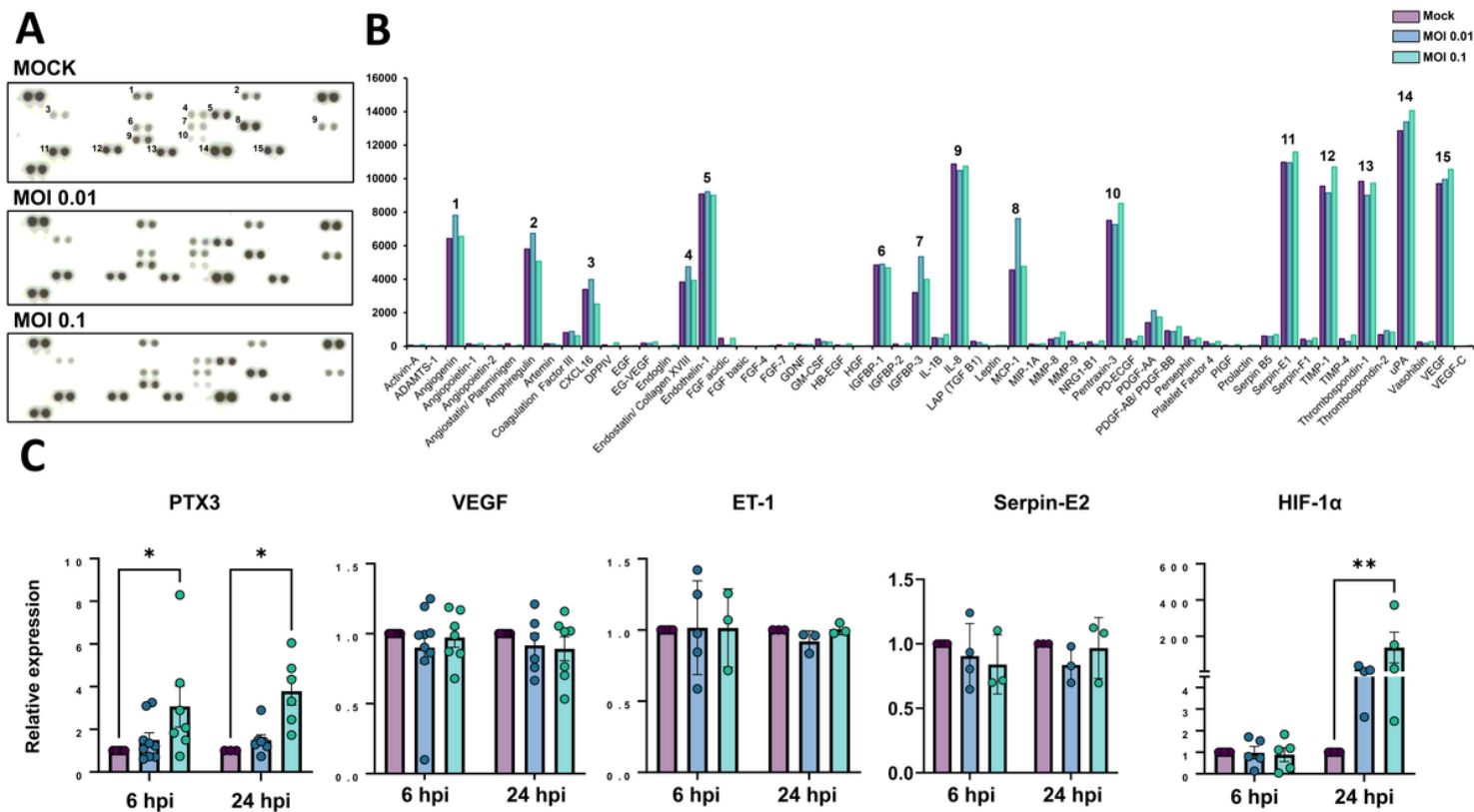
Figure 2

Effects of SARS-CoV-2 on tight junctional proteins in Vero and HBMECs. **A:** Cells were stained for tight junction adaptor protein ZO-1 (red) and SARS-CoV-2 Spike1 (in green). ZO-1 was affected in infected cultures at 24 hpi as shown in higher magnification in the insets. **B**: Morphometrical analyses of ZO-1 fluorescence intensity and TiJOR (D) showed increased ZO-1 signal and TiJOR index at 6 hpi with the MOI 0.01. TJ proteins ZO-1 and Claudin-5 mRNA levels remained unaffected by infection (**C**), but were increased at 24 hpi by MOI 0.1 (**D**). *: $p < 0.05$ One-way ANOVA with Bonferroni post-test (in **D**) or Two-Way ANOVA with Bonferroni post-test (in **B and C**); ****: $p < 0.0001$, Two-Way ANOVA with Bonferroni post-test. Each point in C and D correspond to independent cultures and in **B** correspond to microscopic field from four independent cultures. Representative blots in **D** from three independent experiments.

Figure 3

Transcriptomic profiling of SARS-CoV-2 infection on BBB-forming cells. HBMECs were infected with MOIs 0.01 and 0.1 and analyzed by RNA-Seq. (**A**) Volcano plot depicting the overall profile of differentially expressed genes in cultures infected with MOI 0.1 at 24 hpi, with up-regulated genes shown in purple and down-regulated in green. (**B**) Heatmap diagram depicting expression levels of the most significantly altered genes by MOI 0.1 (3 right columns) as compared to uninfected controls (3 left columns). (**C**) Cnetplot visualization of functional enrichment results with up-regulated genes, depicting the functional correlation of genes with the most significant GO terms. (**D**) Enrichment functional analysis of GO terms most affected by SARS-CoV-2 in HBMECs indicate inflammatory endothelial activation, as well as mitochondrial dysfunction and ribosomal-related gene expression. (**E**) RT-qPCR validation of most significantly altered genes detected in the RNA-Seq indicate activation of non-canonical NF-kB pathway, with massive increase in TNF-α, lymphotoxin B (LTB, or TNF-C) and downstream target genes such as IL-6, CXCL1, -2 and -8. NFKB1 (p105/p50) and NFKB2 (p100/p52) as well as JUNB did not show alteration in infected cultures. *: $p < 0.05$; **: $p < 0.01$; ****: $p < 0.0001$, Two-Way ANOVA with Bonferroni post-test of at least 5 independent experiments. MOI: multiplicity of infection; GO: gene ontology.

Figure 4

Production of angiogenic-related molecules is modulated by SARS-CoV-2 in HBMECs. (A) Conditioned medium from Mock and SARS-CoV-2-infected HBMEC cultures (both with MOI 0.01 and 0.1) were analyzed with Proteome Profiler Human Angiogenic Antibody Array and detected by chemoluminescence, each protein detected in duplicated spots. **(B)** Densitometric analysis of membranes in **A** revealed the analytes with strongest signal and which were affected by infection. **(C)** RT-qPCR analysis of angiogenesis-related genes in HBMECs revealed that PTX3 and HIF-1α were increased in infected cultures. *: $p < 0.05$; **: $p < 0.01$, Two-Way ANOVA with Bonferroni post-test of at least five independent experiments.

Figure 5

SARS-CoV-2-induced mitochondrial remodeling in HBMECs. Mitochondrial networks were detected by TOMM20 immunostaining (**A**) and TEM (**B**). MiNA analysis of TOMM20 revealed that SARS-CoV-2 induced an increase in mitochondrial footprint, branch length mean and summed branch length (**C**). Mitochondrial density was calculated by TEM images (**D**), which also revealed increased fusion and association to multivesicular bodies (**B**). E: RT-qPCR (upper panel) and western blotting (lower panel) analyses revealed that despite fission-related genes (Fis1, Drp1 and MFF) were up-regulated in MOI 0.01-

infected cultures, only Mfn2 protein levels were increased in MOI 0.1-infected cultures. TOMM20 protein levels also remained unaltered. *: p<0.05; **: p<0.01; ***:p<0.001; ****: p<0.0001, Two-way ANOVA with Bonferroni post-test. Each dot in graphs represents one cell (in C), one mitochondrion (in D) or one independent experiment (in E). Bottom right panels depict blots from E. Scale bars: 50 μm for **A** and 500 nm for **B**.

Supplementary Files

This is a list of supplementary files associated with this preprint. Click to download.

- Supplementarymaterial.docx